3D elastic plane-wave diffraction by a stress-free wedge for incident skew angles below the critical angle in diffraction

Samar Chehade, Michel Darmon, Gilles Lebeau

3D elastic plane-wave diffraction by a stress-free wedge for incident skew angles below the critical angle in diffraction

Samar Chehade[a,b,*], Michel Darmon[a,b], Gilles Lebeau[c]

[a] *Université Paris-Saclay, CEA, List, F-91120, Palaiseau, France*
[b] *Université Paris-Saclay, EOBE doctoral school, Espace Technologique Bat. Discovery - RD 128 - 2e ét, 91190 Saint-Aubin, France*
[c] *Laboratoire J.A. Dieudonné, UMR CNRS 7351, Université de Nice Sophia-Antipolis, Parc Valrose, 06108 NICE, France*

Elastic plane wave diffraction by a stress-free wedge is a canonical problem of interest to researchers in many different fields. To our knowledge, no fully analytical resolution has been found and semi-analytical evaluations of asymptotic approximations have therefore become a common approach. In this paper, a method called the spectral functions method is developed in a 3D configuration, meaning that the incident ray is not necessarily in the plane normal to the wedge edge. The diffracted displacement field is expressed as an integral in terms of two unknown functions called the spectral functions. These functions are decomposed into two parts : one which can be computed analytically and the other which is approached numerically using a collocation method. The details of the corresponding numerical scheme are given and first numerical validations are presented. The presented method is valid for incident skew angles which are below the critical angle in diffraction.

1. Introduction

The problem of 3D wedge diffraction has been studied over the past century in acoustics, electromagnetics and in to a lesser degree in elastodynamics. The problem was introduced notably by Sommerfeld [1], who gave an exact expression of the solution to the scattering problem of a scalar plane wave by a wedge with Dirichlet or Neumann boundaries in the form of a contour integral.

In the case of an incident acoustic wave, Rawlins [2] determined an expression of the solution as a real integral for a spherical acoustic wave diffracted by a wedge with Dirichlet or Neumann boundaries when the aperture angle is a multiple of $\frac{\pi}{n}$, where n is an integer. In the case of an electromagnetic wave, Rojas [3] derived a uniform asymptotic solution for a plane wave incident on an impedant wedge when the wedge angle is a multiple of $\frac{\pi}{2}$. Gerard and

Lebeau have studied diffraction by a curved wedge with Dirichlet boundary conditions [4] and their results were generalized to mixed boundary conditions by Lafitte [5]. By generalizing the Malyuzhinets technique [6], Bernard [7] reduced the 3D problem of a plane electromagnetic wave diffracted by an impedance wedge of arbitrary angle to a scalar functional equation with only one unknown and provides examples of numerical resolution of this equation for some particular classes of wedges. In the case of a spherical acoustic wave diffracted by a wedge-shaped separation between two homogeneous mediums, Ayzenberg [8] proposes a numerical scheme of resolution. However, it appears that parallel programming is necessary to obtain a short computation time. To obtain a shorter computation time, some simplifying approximations can be made. Favretto-Cristini [9] studies the effect of these approximations on the resulting accuracy. Finally, an application of the Wiener-Hopf technique to the case of electromagnetic plane wave diffraction by impenetrable wedges of arbitrary angles was developed by Daniele in 2D [10] and extended to 3D cases by Daniele and Lombardi [11]. A review and comparison of various methods and solution forms for acoustic wave diffraction wedge diffraction has been made by Nethercote et al. [12].

In the case of a plane elastic wave, it seems that the solution can not be computed analytically [13]. Therefore, semi-analytical resolutions and far-field ($kr >> 1$, k being the wave number and r being the distance of observation) asymptotics have become common approaches. In this regard, the Geometrical Theory of Diffraction (GTD) was first introduced in electromagnetics by Keller [14]. Sommerfeld's intergral can be used to obtain an analytical expression of the GTD diffraction coefficient both in electromagnetics and in acoustics [15, 16]. In the scalar case of 2D wedge diffraction of a shear horizontally polarized incident wave, a comparison of asymptotic (GTD and uniform) and exact solutions has been carried out in elastodynamics by Aristizabal et al. [17].

The total asymptotic fields obtained with the GTD method does not correctly model all the head waves occuring at the vicinity of a wedge [18] and are spatially non-uniform in the sense that they diverge at shadow boundaries of the Geometrical Elastodynamics (GE) field. Recent developments from the articles [18–23] and a modification [24] of the Kirchhoff approximation has recently been proposed to account for head waves. To solve the divergence problem at shadow boundaries, some uniform corrections of the GTD have been developed. One of these methods is the Physical Theory of Diffraction (PTD), which has been developed in electromagnetics by Ufimtsev [25] and extended to elastic waves [26, 27] but it is computationally expensive for large scatterers. Another uniform correction is the Uniform Asymptotic Theory (UAT) developed in elastodynamics by Achenbach et al. [28]. This method has been tested by Fradkin and Stacey [29], using a finite difference algorithm. It requires an artificial extension of the scattering surface and the construction of fictitious rays [15]. For these reasons, a more commonly used uniform correction of the GTD method is the Uniform Theory of Diffraction (UTD). It was developed in electromagnetics by Kouyoumjian and Pathak [30] and extended to elastodynamics by Kamta Djakou et al. [31], with an application to the scattering from a half-plane. This method is computationally efficient but still requires a trustworthy GTD diffraction model in order to be applied.

In elastodynamics, a GTD solution to the 3D problem of plane wave diffraction by a stress-free half plane was developed by Achenbach and Gautesen [28]. Gautesen [32, 33] also proposed a semi-analytical scheme of resolution of the far-field scattering problem of a skew incident Rayleigh wave diffracted by a quarter-space (i.e. a wedge of angle $\frac{\pi}{2}$ or $\frac{3\pi}{2}$). Budaev also studied the problem of diffraction of a plane wave diffraction by a wedge [34–36] and reduced it to a singular integral equation. However, no clear numerical scheme of resolution has been proposed. Budaev and Bogy [37] have applied this method to the case of an incident Rayleigh wave and have proposed a corresponding numerical resolution. Their theoretical development was incomplete and has been clarified by Kamotski et al. [38]. Budaev and Bogy's method, called the Sommerfeld Integral (SI) method, and Gautesen's method, called the Laplace Transform (LT) method have both been extended by Gautesen and Fradkin [39] to the case of an elastic wave diffracted by a stress-free wedge of angle lower than π. They offer a comparison of the two methods and an experimental validation is given by Chapman et al. [40].

Another boundary integral approach was developed by Croisille and Lebeau [41] in the case of an acoustic plane wave scattered by an immersed elastic wedge. This is called the spectral functions method and was described both theoretically and numerically for the case of an immersed wedge of angle lower than π [41]. In this method, the diffracted displacement field is expressed as an integral in terms of two unknown functions called the spectral functions. These functions are decomposed into two parts : one which can be computed analytically and the other which is approached numerically using a collocation method. In the 2D case of an acoustic wave incident on a soft wedge of arbitrary angle (lower or higher than π), the method has been developed numerically by Chehade et al. [42]. The spectral functions method was also used by Kamotski and Lebeau [43] to prove the existence and uniqueness of the solution to the 2D problem of a plane elastic wave diffracted by a stress free wedge of arbitrary angle. The corresponding numerical

scheme of 2D resolution was given by Chehade et al. [44].

To our knowledge, no resolution scheme has been developed for the 3D problem of a skew incident longitudinal or transversal plane elastic wave diffracted by an arbitrary-angled wedge. Therefore, it is the aim of this article.

In the first part of this paper, the problem is presented. Snell's law for diffraction allows us to define the critical angle in diffraction δ_c, which depends on the propagation medium. For incident transversal waves with skew angles higher than this critical angle, there is no diffracted no diffracted longitudinal wave. In the second part, an integral formulation of the solution is derived, depending on two unknown functions, called the spectral functions. The 3D diffraction coefficient is defined and expressed with respect to these spectral functions. In the third part, the semi-analytical evaluation of these functions is detailed. Finally, the corresponding code is tested numerically in the fourth part.

2. Problem statement

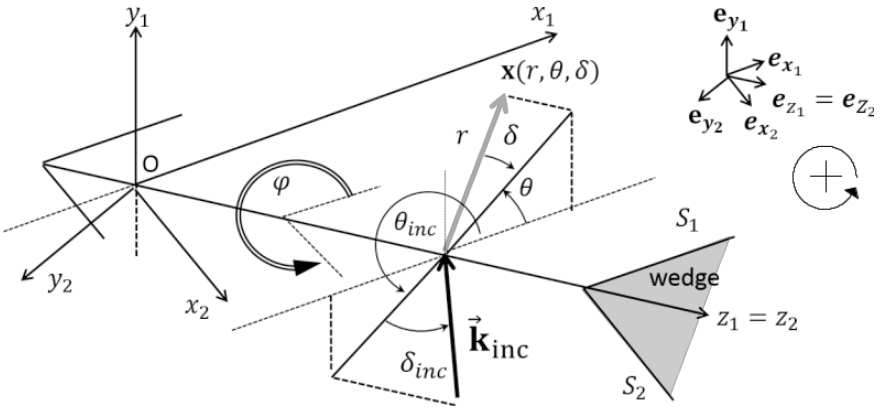

Fig. 1: Geometry of the problem

Let us consider the problem of an elastic wave diffracted by a stress-free infinite wedge delimited by faces $\mathcal{S}_1$ and $\mathcal{S}_2$. The geometry of the problem is shown on Fig. 1. Vector $\mathbf{x} = (r, \theta, \delta)$ is an observation point in the propagation domain indexed by its spherical coordinates and the domain Ω is the inside of the wedge, defined by :

$$\Omega = \{(r\cos\theta\cos\delta, r\sin\theta\cos\delta, r\sin\delta) \setminus \theta \in]0, \varphi[,\ \delta \in]-\frac{\pi}{2}, \frac{\pi}{2}[\} \tag{2.1}$$

The outside of the wedge, in which no wave is propagated, is represented in gray.

The incident wave is a plane wave of the form

$$\mathbf{u}^{inc}(\mathbf{x}, t) = \mathbf{A}_\alpha e^{i(\mathbf{k}_\alpha^{inc}\cdot\mathbf{x} - \omega t)} \tag{2.2}$$

where $\mathbf{A}_\alpha$ is the amplitude vector of the incident wave and $\mathbf{k}_\alpha^{inc}$ is the incident wave vector. The type of the incident wave is denoted by α (α =L for a longitudinal wave, TH for transverse horizontal and TV for transverse vertical). $(O; \mathbf{e}_{x_1}, \mathbf{e}_{y_1}, \mathbf{e}_{z_1})$ is a Cartesian coordinate system associated to face $\mathcal{S}_1$ and $(O; \mathbf{e}_{x_2}, \mathbf{e}_{y_2}, \mathbf{e}_{z_2})$ is a Cartesian coordinate system associated to face $\mathcal{S}_2$. In all the following, vectors are expressed in the coordinate system $\mathbf{x} = (x_1', y_1', z_1')_{(\mathbf{e}_{x_1}, \mathbf{e}_{y_1}, \mathbf{e}_{z_1})}$, unless explicitly mentioned otherwise. In this system, the incident wave vector is given by :

$$\mathbf{k}_\alpha^{inc} = \frac{\omega}{c_\alpha}\begin{pmatrix}\cos\theta_{inc}\cos\delta_{inc}\\ \sin\theta_{inc}\cos\delta_{inc}\\ \sin\delta_{inc}\end{pmatrix} \tag{2.3}$$

$c_L = \sqrt{\underline{\lambda} + 2\underline{\mu}/\rho}$ is the velocity of longitudinal waves and $c_T = \sqrt{\underline{\mu}/\rho}$ is the velocity of transverse waves.

The amplitude vector can be directed by three different two-by-two orthogonal vectors, depending on the incident wave's polarization. These unit polarization vectors are noted $\hat{\imath}_\alpha$, where $\alpha = L, TH, TV$ and are given by Achenbach

[28] :

$$\hat{i}_L = \begin{pmatrix} \cos\theta_{inc}\cos\delta_{inc} \\ \sin\theta_{inc}\cos\delta_{inc} \\ \pm\sin\delta_{inc} \end{pmatrix}, \qquad \hat{i}_{TV} = \begin{pmatrix} \mp\cos\theta_{inc}\sin\delta_{inc} \\ \mp\sin\theta_{inc}\sin\delta_{inc} \\ \cos\delta_{inc} \end{pmatrix}, \qquad \hat{i}_{TH} = \begin{pmatrix} -\sin\theta_{inc} \\ \cos\theta_{inc} \\ 0 \end{pmatrix} \tag{2.4}$$

where the top sign gives the polarization of an incident wave and the bottom sign gives the polarization of a diffracted wave.

For a homogeneous, isotropic material, the linear elasticity equation solved by the displacement field $\mathbf{u}$ is

$$\underline{\mu}\Delta\mathbf{u} + (\underline{\lambda} + \underline{\mu})\nabla\nabla\cdot\mathbf{u} = \rho\frac{\partial^2\mathbf{u}}{\partial t^2} \tag{2.5}$$

On each of the wedge faces, the displacement field verifies the zero-stress boundary conditions, expressed as :

$$(\underline{\lambda}\nabla\cdot\mathbf{u}.\mathbb{I}_{\mathbf{3}} + 2\underline{\mu}\varepsilon(\mathbf{u})).\mathbf{n} = 0 \tag{2.6}$$

where $\mathbb{I}_{\mathbf{3}}$ is the identity matrix of the third order, $\mathbf{n}$ is the inward facing normal to the wedge face ($\mathbf{n} = \mathbf{y}_1$ on $\mathcal{S}_1$ and $\mathbf{n} = \mathbf{y}_2$ on $\mathcal{S}_2$) and $\underline{\lambda}, \underline{\mu}$ are the Lamé coefficients of the considered elastic medium. The deformations tensor is expressed as:

$$\varepsilon(\mathbf{u}) = \frac{1}{2}\begin{pmatrix} 2\dfrac{\partial u_1}{\partial x_1'} & \dfrac{\partial u_1}{\partial y_1'} + \dfrac{\partial u_2}{\partial x_1'} & \dfrac{\partial u_1}{\partial z_1'} + \dfrac{\partial u_3}{\partial x_1'} \\ \dfrac{\partial u_1}{\partial y_1'} + \dfrac{\partial u_2}{\partial x_1'} & 2\dfrac{\partial u_2}{\partial y_1'} & \dfrac{\partial u_2}{\partial z_1'} + \dfrac{\partial u_3}{\partial y_1'} \\ \dfrac{\partial u_1}{\partial z_1'} + \dfrac{\partial u_3}{\partial x_1'} & \dfrac{\partial u_2}{\partial z_1'} + \dfrac{\partial u_3}{\partial y_1'} & 2\dfrac{\partial u_3}{\partial z_1'} \end{pmatrix} \tag{2.7}$$

Kamotski and Lebeau [43] have proven existence and uniqueness of the solution to this problem in the 2D the case. We will assume that this is still true in the 3D case.

In all the following, bold characters will be reserved to matrices in order to simplify notations. The solutions being time harmonic, the factor $e^{-i\omega t}$ will be implied but omitted everywhere. Furthermore, since there is no obstacle to propagation in the z direction, $e^{i\frac{\omega}{c_\alpha}\sin\delta_{inc}z_1'}$ is also a common factor to all the terms which appear in the solution.

The total field is written as the sum of an incident field u^{inc} and a scattered field u_0

$$u = u_0 + u^{inc} \tag{2.8}$$

The dimensionless problem is obtained by applying the following variable change :

$$x = \frac{\omega}{c_L}x', \quad y = \frac{\omega}{c_L}y', \quad z = \frac{\omega}{c_L}z' \tag{2.9a}$$

$$u_0(x', y', z') = \mathrm{v(x,y)e^{-iv_\beta \sin\delta_\beta z}} \tag{2.9b}$$

where β denotes the type of the diffracted wave and δ_β is the angle of Snell's cone of diffraction, visible on Fig. 2 (determined by Snell's law of diffraction, given by (2.12)).

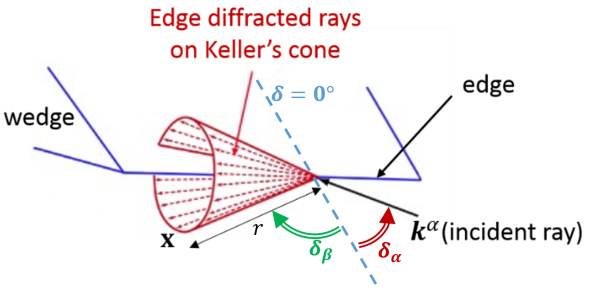

Fig. 2: Keller's cone of diffraction

The dimensionless Lamé parameters λ, μ are defined by

$$\lambda = \frac{\underline{\lambda}}{\rho c_L^2}, \quad \mu = \frac{\underline{\mu}}{\rho c_L^2}, \tag{2.10}$$

and parameters ν_L and ν_T are defined by

$$\nu_L = 1 \qquad \nu_T = \frac{c_L}{c_T} \qquad . \tag{2.11}$$

Since $e^{i\nu_\alpha \sin\delta_{inc} z}$ is a common factor to all the terms of the solution, we can deduce Snell's law of diffraction :

$$\nu_\alpha \sin\delta_{inc} = -\nu_\beta \sin\delta_\beta \tag{2.12}$$

To simplify notations, the following parameter τ is defined by :

$$\tau = \nu_\alpha \sin\delta_{inc} \tag{2.13}$$

Note that we therefore always have $\tau \in [-\nu_\alpha, \nu_\alpha]$. The z-dependency of u_0 is entirely contained in the factor $e^{i\tau z}$ which will be implied but omitted in all the following.

Substituting (2.8) and (2.9) into (2.5) and (2.6) and using (2.7) yields the dimensionless problem

$$(\mathcal{P}^\alpha) \qquad \begin{cases} (E+1)\mathrm{v} = 0 & (\Omega) \\ B\mathrm{v} = -\mathrm{B}\mathrm{v}_\alpha^{\mathrm{inc}} & (\mathcal{S}) \end{cases} \tag{2.14}$$

where E and B are respectively the dimensionless linear elasticity operator and normal stress operator, given by:

$$E\mathrm{v} = \mu(\Delta - \tau^2)\mathrm{v} + (\lambda+\mu)\begin{pmatrix} \frac{\partial^2 \mathrm{v_x}}{\partial x^2} + \frac{\partial^2 \mathrm{v_y}}{\partial x \partial y} + i\tau \frac{\partial \mathrm{v_z}}{\partial x} \\ \frac{\partial^2 \mathrm{v_x}}{\partial x \partial y} + \frac{\partial^2 \mathrm{v_y}}{\partial y^2} + i\tau \frac{\partial \mathrm{v_z}}{\partial y} \\ i\tau\left(\frac{\partial \mathrm{v_x}}{\partial x} + \frac{\partial \mathrm{v_y}}{\partial y}\right) - \tau^2 \mathrm{v_z} \end{pmatrix} \tag{2.15}$$

and, noticing that $\lambda + 2\mu = 1$,

$$B\mathrm{v} = \begin{pmatrix} \mu\left(\frac{\partial \mathrm{v_x}}{\partial y} + \frac{\partial \mathrm{v_y}}{\partial x}\right) \\ \frac{\partial \mathrm{v_y}}{\partial y} + \lambda\left(\frac{\partial \mathrm{v_x}}{\partial x} + i\tau \mathrm{v_z}\right) \\ \mu\left(\frac{\partial \mathrm{v_z}}{\partial y} + i\tau \mathrm{v_y}\right) \end{pmatrix} \tag{2.16}$$

where $(\mathrm{v_x}, \mathrm{v_y}, \mathrm{v_z})$ are the components of vector v. The dimensionless incident field is given by

$$\mathrm{v}_\alpha^{\mathrm{inc}}(\mathrm{r}, \theta) = \mathrm{e}^{\mathrm{i}\mathrm{r}\nu_\alpha \cos(\theta - \theta_{\mathrm{inc}})\cos\delta_{\mathrm{inc}}}\, \hat{\mathrm{i}}_\alpha, \tag{2.17}$$

where vector $\hat{i}_\alpha$ is defined by (2.4). The first equation of system (2.14) is the dimensionless version of the linear elasticity equation and the second equation is the dimensionless version of the stress-free boundary conditions.

3. Integral formulation of the solution

As in the acoustic and elastic 2D cases [42, 44], the first step to solving problem $(\mathcal{P}^\alpha)$ is to formulate the solution as an integral.

3.1. Limiting absorption principle

The limiting absorption principle is applied to $(\mathcal{P}^\alpha)$. This means that it is considered as a special case ($\epsilon = 0$) of the problem

$$(\mathcal{P}_\epsilon^\alpha) \qquad \begin{cases} (E + e^{-2i\epsilon})\mathrm{v}^\epsilon = 0 & (\Omega) \\ B\mathrm{v}^\epsilon = -\mathrm{B}\mathrm{v}_\alpha^{\mathrm{inc}} & (\mathcal{S}) \end{cases} \tag{3.1}$$

Following Kamotski and Lebeau [43], we will assume that the solution can be expressed as the sum of two contributions, corresponding to each of the wedge faces :

$$\mathrm{v}^\epsilon = \mathrm{v}_1^\epsilon + \mathrm{v}_2^\epsilon \tag{3.2}$$

where functions v_j^ϵ are defined on all of $\mathbb{R}^3$ by

$$v_j^\epsilon = -(E + e^{-2i\epsilon})^{-1} \left[\begin{pmatrix} \alpha_j \\ \beta_j \\ \gamma_j \end{pmatrix} \otimes \delta_{\mathcal{S}_j} \right] \tag{3.3}$$

Distributions $\alpha_j, \beta_j, \gamma_j$ are unknown and belong to the special class $\mathcal{A}$ defined by Kamotski and Lebeau [43] as:

Def. 3.1. *The distribution $f \in \mathcal{A}$ if:*

- $f \in \mathcal{S}'(\mathbb{R})$ *(f is a tempered distribution)*
- $supp(f) \subset [0, +\infty[$
- $\exists C_0 > 0$ *such that*

$$\sup_{-\pi<\theta<0} \int_{\rho>C_0} |\hat{f}\left(\rho e^{i\theta}\right)| \, d\rho < \infty$$

  where $\hat{f}$ is the Fourier transform of f defined by $\hat{f}(\xi) = \int_{\mathbb{R}} f(x) e^{-ix\xi} \, dx$

- $\hat{f}(\xi)$ *is holomorphic near* $\xi = 1$

We can now define the outgoing solution of $(\mathcal{P}^\alpha)$ analogously to the 2D case :

Def. 3.2. *v is called an outgoing solution of equation* (2.14) *if v is a solution of the form*

$$v = v_1|_\Omega + v_2|_\Omega \tag{3.4}$$

where, for $j = 1, 2$:

$$v_j = -\lim_{\epsilon \to 0} (E + e^{-2i\epsilon})^{-1} \left[\begin{pmatrix} \alpha_j \\ \beta_j \\ \gamma_j \end{pmatrix} \otimes \delta_{\mathcal{S}_j} \right] \tag{3.5}$$

where $\alpha_j, \beta_j, \gamma_j \in \mathcal{A}$ and where $\delta_{\mathcal{S}_1}$ and $\delta_{\mathcal{S}_2}$ are the Dirac distributions associated to the wedge faces $\mathcal{S}_1$ and $\mathcal{S}_2$ respectively.

The following theorem was proven by Kamotski and Lebeau [43] in the 2D case. Demonstrating that their work can be adapted to the 3D case is a complex problem which would require a separate publication. We will therefore simply assume that this is the case and that the following theorem is still true.

Theorem 3.1. *Equation* (2.14) *admits a unique outgoing solution.*

Now that the outgoing solution has been defined, we will derive an integral formulation of this solution.

3.2. Integral formulation

The two-sided Fourier transform of a tempered distribution and its inverse are defined in the following manner :

$$\hat{f}(\xi, \eta) = \int \int_{\mathbb{R}^2} f(x, y) e^{-i(x\xi + y\eta)} \, \mathrm{d}x\mathrm{d}y \tag{3.6a}$$

$$f(x, y) = \frac{1}{4\pi^2} \int \int_{\mathbb{R}^2} \hat{f}(\xi, \eta) e^{i(x\xi + y\eta)} \mathrm{d}\xi\mathrm{d}\eta \tag{3.6b}$$

The first step in determining an integral formulation of the solution is to apply the two-sided Fourier transform to (3.3). This is possible because all the distributions that appear in this equation are tempered distributions and they therefore admit a Fourier transform. We then have :

$$\hat{v}_j^\epsilon(\xi, \eta) = (\mathbf{M} - e^{-2i\epsilon} \mathbb{I}_\mathbf{3})^{-1} \Sigma_j(\xi), \tag{3.7}$$

where Σ_j, $j = 1, 2$ are the unknown spectral functions, defined by :

$$\Sigma_j(\xi) = \begin{pmatrix} \hat{\alpha}_j(\xi) \\ \hat{\beta}_j(\xi) \\ \hat{\gamma}_j(\xi) \end{pmatrix} \tag{3.8}$$

and where $\mathbf{M}$ is the two-sided Fourier transform of operator E. Its expression is :

$$\mathbf{M}(\xi,\eta) = \begin{pmatrix} \xi^2 + \mu(\eta^2+\tau^2) & (\lambda+\mu)\xi\eta & (\lambda+\mu)\xi\tau \\ (\lambda+\mu)\xi\eta & \eta^2 + \mu(\xi^2+\tau^2) & (\lambda+\mu)\eta\tau \\ (\lambda+\mu)\xi\tau & (\lambda+\mu)\eta\tau & \tau^2 + \mu(\xi^2+\eta^2) \end{pmatrix} \tag{3.9}$$

Substituting λ by $1-2\mu$ and μ by $1/\nu_T^2$ in (3.9) yields

$$(\mathbf{M} - e^{-2i\epsilon}\mathbb{I}_3)^{-1} = \frac{\begin{pmatrix} \xi^2 + \nu_T^2(\eta^2+\tau^2-e^{-2i\epsilon}) & (1-\nu_T^2)\xi\eta & (1-\nu_T^2)\xi\tau \\ (1-\nu_T^2)\xi\eta & \eta^2 + \nu_T^2(\xi^2+\tau^2-e^{-2i\epsilon}) & (1-\nu_T^2)\tau\eta \\ (1-\nu_T^2)\xi\tau & (1-\nu_T^2)\tau\eta & \tau^2 + \nu_T^2(\eta^2+\xi^2-e^{-2i\epsilon}) \end{pmatrix}}{(\xi^2+\eta^2+\tau^2-e^{-2i\epsilon})(\xi^2+\eta^2+\tau^2-\nu_T^2 e^{-2i\epsilon})} \tag{3.10}$$

Finally, the integral formulation of $\mathrm{v_j}$ is obtained by inverting the two-sided Fourier transform applied in (3.7) :

$$\mathrm{v_j^\epsilon}(\mathrm{x_j},\mathrm{y_j}) = \frac{1}{4\pi^2}\int_{\mathbb{R}^2} \mathrm{e^{ix_j\xi}}\left(\int_{-\infty}^{+\infty} \mathrm{e^{iy_j\eta}}(\mathbf{M} - \mathrm{e^{-2i\epsilon}}\mathbb{I}_\mathbf{3})^{-1}\,\mathrm{d}\eta\right)\Sigma_\mathrm{j}(\xi)\,\mathrm{d}\xi \tag{3.11}$$

The poles of $(\mathbf{M} - e^{-2i\epsilon}\mathbb{I}_\mathbf{3})^{-1}$ (which are the poles of the integrand of the inner integral on η in (3.11)) are located at $\eta = \pm\zeta_*^\epsilon(\xi)$ according to (3.10), where $* = L, T$ and

$$\zeta_*^\epsilon(\xi) = \sqrt{e^{-2i\epsilon}\nu_*^2 - (\xi^2+\tau^2)} \tag{3.12}$$

Let us define $\tilde{\nu}_*, * = L, T$ by

$$\tilde{\nu}_*^\epsilon = \sqrt{e^{-2i\epsilon}\nu_*^2 - \tau^2} \tag{3.13}$$

If the incident wave is longitudinal, then, according to (2.13), $\tau = \sin\delta_{inc}$ and

$$\tilde{\nu}_L^0 = \sqrt{1-\sin^2\delta_{inc}} = \cos\delta_{inc} \quad \in \mathbb{R} \tag{3.14a}$$

$$\tilde{\nu}_T^0 = \sqrt{\nu_T^2 - \sin^2\delta_{inc}} \quad \in \mathbb{R}, \tag{3.14b}$$

since $\nu_L = 1$ and $\nu_T = \frac{c_L}{c_T} > 1$. However, if the incident wave is transverse, then $\tau = \nu_T \sin\delta_{inc}$ and we have

$$\tilde{\nu}_T^0 = \sqrt{\nu_T^2 - \nu_T^2\sin^2\delta_{inc}} = \nu_T\cos\delta_{inc} \quad \in \mathbb{R}, \tag{3.15}$$

and for $\tilde{\nu}_L^0$, two cases may occur :

- if $|\sin\delta_{inc}| \leq \dfrac{\nu_L}{\nu_T}$, then $\tilde{\nu}_L^0 = \sqrt{1-\nu_T^2\sin^2\delta_{inc}} \quad \in \mathbb{R}$ (3.16)
- if $|\sin\delta_{inc}| > \dfrac{\nu_L}{\nu_T}$, then $\tilde{\nu}_L^0 = \sqrt{1-\nu_T^2\sin^2\delta_{inc}} = i\sqrt{\nu_T^2\sin^2\delta_{inc}-1} \quad \in i\mathbb{R}$ (3.17)

In the case described by (3.17), the presence of an imaginary branch point considerably complicates all complex integral contour deformations used in the sequel. Some ideas on how to deal with this in practice are proposed in [45], but a theoretical solution has yet to be found. In this paper, we will only deal with the case described by (3.16) and we will hereon after assume that $\tilde{\nu}_L \in \mathbb{R}$, which implies that the skew incident angle is smaller than a certain critical angle δ_c. Physically, if we define a critical angle for diffraction δ_c by $\sin\delta_c = \frac{\nu_L}{\nu_T}$, then the case described in (3.16) corresponds to the case where the incident skew angle (the angle between the incident wave vector and the plane

normal to the wedge edge) is lower than the critical angle. On the contrary, the case described by (3.17) corresponds to the case where the incident skew angle is higher than this critical angle and, according to Snell's law of diffraction (2.12), there is no diffracted longitudinal wave. Going back to the poles ζ_*^ϵ given by (3.12), and substituting the definition on $\tilde{\nu}_*^\epsilon$ (3.13) we have:

$$\zeta_*^\epsilon(\xi) = \sqrt{(\tilde{\nu}_*^\epsilon)^2 - \xi^2} \tag{3.18}$$

The inner integral of (3.11) is computed using Cauchy's residue theorem. The first step in doing so is to compute the eigen vectors and eigen values of $\mathbf{M}$. The three eigenvectors of $\mathbf{M}$ and their corresponding eigenvalues are :

$$\mathbf{M}\begin{pmatrix}\xi\\ \eta\\ \tau\end{pmatrix} = (\xi^2+\eta^2+\tau^2)\begin{pmatrix}\xi\\ \eta\\ \tau\end{pmatrix} \tag{3.19a}$$

$$\mathbf{M}\begin{pmatrix}-\eta\\ \xi\\ 0\end{pmatrix} = \frac{\xi^2+\eta^2+\tau^2}{\nu_T^2}\begin{pmatrix}-\eta\\ \xi\\ 0\end{pmatrix} \tag{3.19b}$$

$$\mathbf{M}\begin{pmatrix}-\xi\tau\\ \eta\tau\\ \xi^2+\eta^2\end{pmatrix} = \frac{\xi^2+\eta^2+\tau^2}{\nu_T^2}\begin{pmatrix}-\xi\tau\\ \eta\tau\\ \xi^2+\eta^2\end{pmatrix} \tag{3.19c}$$

These three vectors are linearly independent and constitute a vector basis of $\mathbb{C}^3$. This means that any vector of $\mathbb{C}^3$ can be expressed as a linear combination of these three vectors. In particular:

$$\Sigma_j = \begin{pmatrix}\hat{\alpha}_j\\ \hat{\beta}_j\\ \hat{\gamma}_j\end{pmatrix} = \frac{\xi\hat{\alpha}_j+\eta\hat{\beta}_j+\tau\hat{\gamma}_j}{\xi^2+\eta^2+\tau^2}\begin{pmatrix}\xi\\ \eta\\ \tau\end{pmatrix} + \frac{\xi\hat{\beta}_j-\eta\hat{\alpha}_j}{\xi^2+\eta^2}\begin{pmatrix}-\eta\\ \xi\\ 0\end{pmatrix} + \frac{(\xi^2+\eta^2)\hat{\gamma}_j-\tau(\xi\hat{\alpha}_j+\eta\hat{\beta}_j)}{(\xi^2+\eta^2)(\xi^2+\eta^2+\tau^2)}\begin{pmatrix}-\xi\tau\\ \eta\tau\\ \xi^2+\eta^2\end{pmatrix} \tag{3.20}$$

This allows us to write the term $(\mathbf{M}-e^{-2i\epsilon}\mathbb{I}_3)^{-1}\Sigma_j$ as the sum of three contributions :

$$\begin{aligned}(\mathbf{M}-e^{-2i\epsilon}\mathbb{I}_3)^{-1}\Sigma_j = {}& \frac{\xi\hat{\alpha}_j+\eta\hat{\beta}_j+\tau\hat{\gamma}_j}{\xi^2+\eta^2+\tau^2}[(\xi^2+\eta^2+\tau^2)-e^{-2i\epsilon}]^{-1}\begin{pmatrix}\xi\\ \eta\\ \tau\end{pmatrix}\\ &+ \frac{\xi\hat{\beta}_j-\eta\hat{\alpha}_j}{\xi^2+\eta^2}[\frac{\xi^2+\eta^2+\tau^2}{\nu_T^2}-e^{-2i\epsilon}]^{-1}\begin{pmatrix}-\eta\\ \xi\\ 0\end{pmatrix}\\ &+ \frac{(\xi^2+\eta^2)\hat{\gamma}_j-\tau(\xi\hat{\alpha}_j+\eta\hat{\beta}_j)}{(\xi^2+\eta^2)(\xi^2+\eta^2+\tau^2)}[\frac{\xi^2+\eta^2+\tau^2}{\nu_T^2}-e^{-2i\epsilon}]^{-1}\begin{pmatrix}-\xi\tau\\ \eta\tau\\ \xi^2+\eta^2\end{pmatrix}\end{aligned} \tag{3.21}$$

Expression (3.21) therefore simplifies the evaluation of the residues of the integral on η in (3.11) at poles $\pm\zeta_*^\epsilon(\xi)$, yielding

$$\mathrm{v_j^\epsilon}(\mathrm{x_j},\mathrm{y_j}) = \frac{\mathrm{i}}{4\pi}\mathrm{e}^{2\mathrm{i}\epsilon}\int_{\mathbb{R}}\mathrm{e}^{\mathrm{i}\mathrm{x_j}\xi}\sum_{*=\mathrm{L,TH,TV}}\mathrm{e}^{\mathrm{i}|\mathrm{y_j}|\zeta_*^\epsilon(\xi)}\mathbf{M}_*^\epsilon(\xi,\mathrm{sgn}\ \mathrm{y_j})\Sigma_\mathrm{j}(\xi)\,\mathrm{d}\xi \tag{3.22}$$

where $\mathbf{M}_*^\epsilon(\xi,t), * = L, TH, TV$ are defined by

$$\mathbf{M}_\mathbf{L}^\epsilon(\xi,t) = \begin{pmatrix}\frac{\xi^2}{\zeta_L^\epsilon} & t\xi & \frac{\xi\tau}{\zeta_L^\epsilon}\\ t\xi & \zeta_L^\epsilon & t\tau\\ \frac{\xi\tau}{\zeta_L^\epsilon} & t\tau & \frac{\tau^2}{\zeta_L^\epsilon}\end{pmatrix} \tag{3.23a}$$

$$\mathbf{M}_\mathbf{TV}^\epsilon(\xi,t) = \begin{pmatrix}\frac{\xi^2\tau^2}{\zeta_T^\epsilon(\xi^2+\zeta_T^{\epsilon 2})} & \frac{t\xi\tau^2}{\xi^2+\zeta_T^{\epsilon 2}} & \frac{-\xi\tau}{\zeta_T^\epsilon}\\ \frac{t\xi\tau^2}{\xi^2+\zeta_T^{\epsilon 2}} & \frac{\zeta_T^\epsilon\tau^2}{\xi^2+\zeta_T^{\epsilon 2}} & -t\tau\\ \frac{-\xi\tau}{\zeta_T^\epsilon} & -t\tau & \frac{\xi^2+\zeta_T^{\epsilon 2}}{\zeta_T^\epsilon}\end{pmatrix} \tag{3.23b}$$

$$\mathbf{M}^{\epsilon}_{\mathbf{TH}}(\xi,t)=\left(1+\frac{\tau^2}{\xi^2+\zeta_T^{\epsilon 2}}\right)\begin{pmatrix}\zeta_T^{\epsilon} & -t\xi & 0\\ -t\xi & \frac{\xi^2}{\zeta_T^{\epsilon}} & 0\\ 0 & 0 & 0\end{pmatrix} \tag{3.23c}$$

In order to simplify notations, let us define $\mathbf{M}^{\epsilon}_{\mathbf{T}}=\mathbf{M}^{\epsilon}_{\mathbf{TH}}+\mathbf{M}^{\epsilon}_{\mathbf{TV}}$,

$$\mathbf{M}^{\epsilon}_{\mathbf{T}}(\xi,t)=\begin{pmatrix}\zeta_T^{\epsilon}+\frac{\tau^2}{\zeta_T^{\epsilon}} & -t\xi & -\frac{\xi\tau}{\zeta_T^{\epsilon}}\\ -t\xi & \frac{\xi^2+\tau^2}{\zeta_T^{\epsilon}} & -t\tau\\ -\frac{\xi\tau}{\zeta_T^{\epsilon}} & -t\tau & \zeta_T^{\epsilon}+\frac{\xi^2}{\zeta_T^{\epsilon}}\end{pmatrix} \tag{3.24}$$

Integral (3.22) is well defined for $\mathrm{Im}\zeta_*^{\epsilon}>0$, so that the exponential in the integral decreases with the distance y_j. The branch cut for the square root in the definition of ζ_*^{ϵ} (3.18) is therefore:

$$\zeta_*^{\epsilon}=\begin{cases} i\sqrt{\xi^2-\tilde{\nu}_*^{\epsilon 2}} & \text{if} \quad |\xi|\geq|\tilde{\nu}_*^{\epsilon}|\\ -\sqrt{\tilde{\nu}_*^{\epsilon 2}-\xi^2} & \text{if} \quad |\xi|<|\tilde{\nu}_*^{\epsilon}|\end{cases} \tag{3.25}$$

For values of $\epsilon\in]0,\pi[$, the integration contour (real axis) of (3.22) never crosses the branch points of ζ_*^{ϵ}, which are located at $\pm\tilde{\nu}_*^{\epsilon}$ ($\tilde{\nu}_*^{\epsilon}$ is given by (3.13)), outside of the real axis.

According to Croisille et Lebeau [41], convergence in the 2D case is verified for $\epsilon\to 0$. We will assume that this is still true in 3D. The integration contour $\mathbb{R}$ is deformed into contour Γ_0, visible on Fig. 3.

In all the following, superscript $\epsilon=0$ will be omitted in order to alleviate notations. Finally:

$$\mathrm{v_j}(\mathrm{x_j},\mathrm{y_j})=\frac{\mathrm{i}}{4\pi}\int_{\Gamma_0}\mathrm{e}^{\mathrm{i}x_j\xi}\sum_{*=\mathrm{L,T}}\mathrm{e}^{\mathrm{i}|y_j|\zeta_*(\xi)}\mathbf{M}_*(\xi,\mathrm{sgn\ y_j})\Sigma_j(\xi)\,\mathrm{d}\xi \tag{3.26}$$

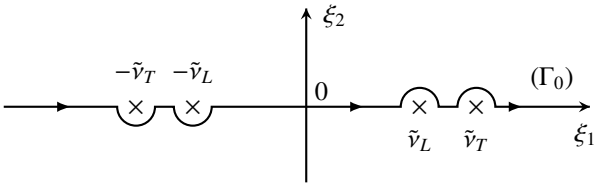

Fig. 3: Contour Γ_0 in the complex plane $\xi=\xi_1+i\xi_2$

Integral formulation (3.26) is an expression of the solution in terms of the unknown spectral function Σ_j. In the next section, a far-field approximation of this integral is derived and the diffraction coefficient is defined.

3.3. Far field approximation

$P=(x_1',y_1',z_1')=(r\cos\theta\cos\delta_\beta, r\sin\theta\cos\delta_\beta, -r\sin\delta_\beta)$ is an observation point, indexed by its spherical coordinates, visible on Fig. 1. In order for the diffracted field to be observable at this point, x is located on one of Keller's cones of diffraction, visible on Fig. 2. The observation skew angle δ_β is set by Snell's law of diffraction (2.12).

According to (2.9), the scattered field at point P is :

$$u_0(x_1',y_1',z_1')=v(\frac{\omega}{c_L}r\cos\theta\cos\delta_\beta,\frac{\omega}{c_L}r\sin\theta\cos\delta_\beta)e^{-ik_\beta\sin\delta_\beta z_1'} \tag{3.27}$$

The far field parameter is $R=\frac{\omega r}{c_L}$. The aim is to determine the asymptotic behavior of $v(R\cos\theta\cos\delta_\beta, R\sin\theta\cos\delta_\beta)$ when $R\to+\infty$. The first step is to apply the following change of variables in integral (3.26):

$$\begin{aligned}\xi&=\tilde{\nu}_*\cos\psi\\ d\xi&=-\tilde{\nu}_*\sin\psi\,d\psi\end{aligned} \tag{3.28}$$

yielding

$$\mathrm{v_1}(\mathrm{r},\theta,\delta_\beta)=\frac{\mathrm{i}}{4\pi}\int_{\mathrm{C_0}}\sum_{*=\mathrm{L,T}}\tilde{\nu}_*^2\mathrm{e}^{\mathrm{i}\tilde{\nu}_*\mathrm{R}\cos\delta_\beta\cos(\psi+\bar{\theta})}\mathbf{P}_*(\psi,\mathrm{t})\Sigma_1(\tilde{\nu}_*\cos\psi)\,\mathrm{d}\psi \tag{3.29}$$

where $\bar{\theta}$ is defined by

$$\bar{\theta} = \begin{cases} \theta & \text{if } \theta \leq \pi \\ 2\pi - \theta & \text{if } \theta > \pi \end{cases}, \tag{3.30}$$

and

$$\mathbf{P_L}(\psi, t) = \begin{pmatrix} \cos^2\psi & -t\cos\psi\sin\psi & \frac{\tau}{\tilde{\nu}_L}\cos\psi \\ -t\cos\psi\sin\psi & \sin^2\psi & -t\frac{\tau}{\tilde{\nu}_L}\sin\psi \\ \frac{\tau}{\tilde{\nu}_L}\cos\psi & -t\frac{\tau}{\tilde{\nu}_L}\sin\psi & \frac{\tau^2}{\tilde{\nu}_L^2} \end{pmatrix} \tag{3.31a}$$

$$\mathbf{P_T}(\psi, t) = \begin{pmatrix} \sin^2\psi + \frac{\tau^2}{\tilde{\nu}_T^2} & t\cos\psi\sin\psi & -\frac{\tau}{\tilde{\nu}_T}\cos\psi \\ t\cos\psi\sin\psi & \cos^2\psi + \frac{\tau^2}{\tilde{\nu}_T^2} & t\frac{\tau}{\tilde{\nu}_T}\sin\psi \\ -\frac{\tau}{\tilde{\nu}_T}\cos\psi & t\frac{\tau}{\tilde{\nu}_T}\sin\psi & 1 \end{pmatrix}, \tag{3.31b}$$

where $t = \operatorname{sgn}\sin\theta$ and contour C_0 is visible on Fig. 4. Note that contour C_0 does not exactly follow $\psi_1 = \pi$. This corresponds to adding an infinitely small imaginary part to the axis Γ_0 represented in Fig. 3, in order to avoid the branch points $\xi = \pm\tilde{\nu}_*$ located at $\psi = 0$ and $\psi = \pi$, where ψ is given by (3.28).

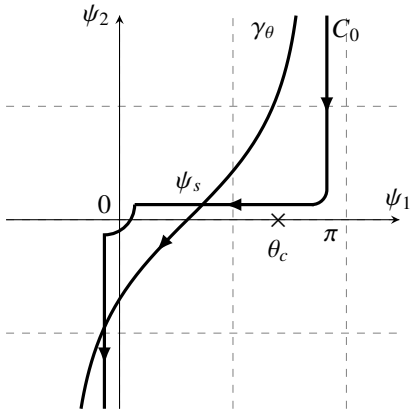

Fig. 4: Contour C_0 and γ_θ in the complex plane $\psi = \psi_1 + i\psi_2$. The stationary phase points are noted ψ_s and θ_c is the critical angle in reflection.

The far-field evaluation of integral (3.29) is obtained by applying the steepest descent method to it. To do so, contour C_0 is deformed into contour γ_θ, also visible in Fig. 4. This leads to

$$\mathrm{v_j} = \mathrm{v_j^{sing}} + \mathrm{v_j^{diff}} \tag{3.32}$$

where $\mathrm{v_j^{sing}}$ is the contribution of all the singularities of the spectral functions crossed during the deformation from C_0 to γ_θ, corresponding to the reflected waves (for the poles of the spectral functions) and head waves (for the branch points ψ_c of the function $\mathrm{v_1}$), and $\mathrm{v_j^{diff}}$ is the contribution of the stationary phase point $\psi_s = \pi - \bar{\theta}$. In the following, it is assumed that the saddle point ψ_s does not coalesce with a branch point. The branch points of functions $\mathrm{v_j}$, $\mathrm{j} = 1, 2$ are located at $\xi = \pm\tilde{\nu}_L$ and $\xi = \pm\tilde{\nu}_T$. Applying (3.28), this means that :

$$\tilde{\nu}_* \cos\psi_s = -\tilde{\nu}_* \cos\theta = \pm\tilde{\nu}_L \tag{3.33a}$$

$$\text{or} \quad \tilde{\nu}_* \cos\psi_\mathrm{s} = -\tilde{\nu}_* \cos\theta = \pm\tilde{\nu}_\mathrm{T} \tag{3.33b}$$

For $* = L$, (3.33a) yields $\theta = 0$ or $\theta = \pi$, meaning that the direction of observation is grazing along the wedge's face $\mathcal{S}_j$. (3.33b) does not have a real solution for $* = L$. For $* = T$, (3.33a) yields $\theta = \theta_c = \operatorname{acos}(\tilde{\nu}_\mathrm{L}/\tilde{\nu}_\mathrm{T})$ or $\theta = \pi - \theta_c$, where θ_c is called the critical angle for reflection and corresponds to the diffracted bulk transverse component of the head wave [18], and (3.33b) yields $\theta = 0$ or $\theta = \pi$, which corresponds to a grazing observation direction along face $\mathcal{S}_j$. Borovikov [46] gives some clues as to how to treat the case where the stationary phase point coincides with another singularity of the integrand but no high-frequency asymptotics prove satisfactory in some situations of practical interest [47] and are not available when the critical transition zones overlap penumbras, that is when

all three critical points (stationary, branch and pole) coalesce [48]. In the present work, only the stationary phase contribution corresponding to the edge-diffracted waves will be computed. In order to simplify notations, we will note $\mathbf{P}_*(\psi, 1) = \mathbf{P}_*(\psi)$, using the fact that $t = \pm 1$ and $\mathbf{P}_*(\psi, -1) = \mathbf{P}_*(-\psi)$. The contribution of diffracted waves is

$$\mathrm{v}_1^{\mathrm{diff}}(\mathrm{r}, \theta, \delta_\beta) = \frac{\mathrm{e}^{-\mathrm{i}\pi/4}}{2\sqrt{2\pi}} \sum_{*=\mathrm{L,T}} \tilde{\nu}_*^2 \frac{\mathrm{e}^{-\mathrm{i}\tilde{\nu}_* \mathrm{R}\cos\delta_\beta}}{\sqrt{\tilde{\nu}_* R \cos\delta_\beta}} \mathbf{P}_*(\pi - \theta)\Sigma_1(-\tilde{\nu}_* \cos\theta) \tag{3.34}$$

Analogously,

$$\mathrm{v}_2^{\mathrm{diff}}(\mathrm{r}, \varphi - \theta, \delta_\beta) = \frac{\mathrm{e}^{-\mathrm{i}\pi/4}}{2\sqrt{2\pi}} \sum_{*=\mathrm{L,T}} \tilde{\nu}_*^2 \frac{\mathrm{e}^{-\mathrm{i}\tilde{\nu}_* \mathrm{R}\cos\delta_\beta}}{\sqrt{\tilde{\nu}_* R \cos\delta_\beta}} \mathbf{P}_*(\pi - (\varphi - \theta))\Sigma_1(-\tilde{\nu}_* \cos(\varphi - \theta)) \tag{3.35}$$

Let us now isolate L, TH and TV diffracted waves in order to compute the corresponding diffraction coefficients, defined by

$$\mathrm{v}_\beta^{\mathrm{diff}}(\mathrm{r}, \theta, \delta_\beta) = \mathrm{D}_\beta^\alpha(\theta) \frac{\mathrm{e}^{-\mathrm{i}\tilde{\nu}_\beta \mathrm{R}\cos\delta_\beta}}{\sqrt{\tilde{\nu}_\beta R \cos\delta_\beta}} \mathrm{v}^{\mathrm{inc}}(\mathrm{r}\cos\theta, \mathrm{r}\sin\theta)\hat{\mathrm{i}}_\beta, \tag{3.36}$$

using the expressions of the unit vectors given by (2.4). This yields:

$$D_\beta^\alpha(\theta) = \frac{e^{-i\pi/4}}{2\sqrt{2\pi}} \sum_{j=1,2} \tilde{\nu}_\beta^2 \left\langle \left(\mathbf{P}_\beta(\pi - \theta_j) \cdot \hat{\imath}_\beta\right), \Sigma_j(-\tilde{\nu}_\beta \cos\theta_j)\right\rangle \tag{3.37}$$

where $\theta_1 = \theta$ and $\theta_2 = \varphi - \theta$ and $\langle \cdot, \cdot \rangle$ denotes the dot product of two vectors.

In a far-field approximation, in order to determine the field diffracted by a wedge illuminated by an incident plane wave, it is sufficient to compute the diffraction coefficient. This coefficient has been expressed in terms of two unknown functions called the spectral functions. The semi-analytical computation of these functions is presented in the following section

4. Semi-analytical evaluation of the spectral functions

The first step in computing the spectral functions is to determine a system of functional equations of which they are a solution. We will then show that these functions can be decomposed into two parts : a singular function, computed analytically, and a regular function, approached numerically.

4.1. Functional equations

In the previous section, the diffracted wave has been expressed in terms of two unknown functions called the spectral functions. In this subsection, a system of functional equations satisfied by these functions is determined.

The first step in determining a system of functional equations verified by the spectral functions, is to substitute decomposition (3.2) into the boundary conditions :

$$\begin{cases} B(\mathrm{v}_1(\mathrm{x}_1, 0) + \mathrm{v}_2(\mathrm{x}_2\cos\varphi, \mathrm{x}_2\sin\varphi)) = -\mathrm{B}\mathrm{v}_\alpha^{\mathrm{inc}}|_{\mathcal{S}_1} \\ B(\mathrm{v}_2(\mathrm{x}_2, 0) + \mathrm{v}_1(\mathrm{x}_1\cos\varphi, \mathrm{x}_1\sin\varphi)) = -\mathrm{B}\mathrm{v}_\alpha^{\mathrm{inc}}|_{\mathcal{S}_2} \end{cases} \tag{4.1}$$

Let us note $(\mathrm{v}_\mathrm{j}^1, \mathrm{v}_\mathrm{j}^2, \mathrm{v}_\mathrm{j}^3)$ the coordinates of v_j in the Cartesian coordinate system (x_j, y_j, z_j), where (x_1, y_1, z_1) is the coordinate system associated with face $\mathcal{S}_1$ and (x_2, y_2, z_2) is the coordinate system associated with face $\mathcal{S}_2$. These two coordinate systems are linked by (for $j = 1, 2$):

$$\begin{cases} x_j = \cos\varphi.x_{3-j} + \sin\varphi.y_{3-j} \\ y_j = \sin\varphi.x_{3-j} - \cos\varphi.y_{3-j} \\ z_j = z_{3-j} \end{cases} \tag{4.2}$$

Applying (4.2) to each line of (4.1) yields:

$$\begin{cases} B_1(\mathrm{v}_1) + \mathrm{B}_2(\mathrm{v}_2) = -\mathrm{B}\mathrm{v}_\alpha^{\mathrm{inc}}|_{\mathcal{S}_1} \\ B_1(\mathrm{v}_2) + \mathrm{B}_2(\mathrm{v}_1) = -\mathrm{B}\mathrm{v}_\alpha^{\mathrm{inc}}|_{\mathcal{S}_2} \end{cases} \tag{4.3}$$

where

$$B_1(\mathrm{v}) = \begin{pmatrix} \mu\left(\frac{\partial \mathrm{v_x}}{\partial y_1} + \frac{\partial \mathrm{v_y}}{\partial x_1}\right) \\ \frac{\partial \mathrm{v_y}}{\partial y_1} + \lambda\left(\frac{\partial \mathrm{v_x}}{\partial x_1} + \frac{\partial \mathrm{v_z}}{\partial z_1}\right) \\ \mu\left(\frac{\partial \mathrm{v_y}}{\partial z_1} + \frac{\partial \mathrm{v_z}}{\partial y_1}\right) \end{pmatrix} \tag{4.4}$$

and

$$B_2(\mathrm{v}) = \begin{pmatrix} \mu\sin(2\varphi)\left(\frac{\partial \mathrm{v_x}}{\partial x_2} - \frac{\partial \mathrm{v_y}}{\partial y_2}\right) - \mu\cos(2\varphi)\left(\frac{\partial \mathrm{v_x}}{\partial y_2} + \frac{\partial \mathrm{v_y}}{\partial x_2}\right) \\ (\lambda + 2\mu\sin^2\varphi)\frac{\partial \mathrm{v_x}}{\partial x_2} + (\lambda + 2\mu\cos^2\varphi)\frac{\partial \mathrm{v_y}}{\partial y_2} - \mu\sin(2\varphi)\left(\frac{\partial \mathrm{v_x}}{\partial y_2} + \frac{\partial \mathrm{v_y}}{\partial x_2}\right) + \lambda\frac{\partial \mathrm{v_z}}{\partial z_2} \\ \mu\sin\varphi\left(\frac{\partial \mathrm{v_z}}{\partial x_2} + \frac{\partial \mathrm{v_x}}{\partial z_2}\right) - \mu\cos\varphi\left(\frac{\partial \mathrm{v_y}}{\partial z_2} + \frac{\partial \mathrm{v_z}}{\partial y_2}\right) \end{pmatrix} \tag{4.5}$$

Operator B_1 is obtained by projecting $B(\mathrm{v}_1)$ onto $\mathcal{S}_1$. This is immediate because v_1 is defined on $\mathcal{S}_1$ and its components $(\mathrm{v}_1^1, \mathrm{v}_1^2, \mathrm{v}_1^3)$ are expressed in the associated Cartesian coordinate system (x_1, y_1, z_1). Operator B_2 is obtained by projecting $B(\mathrm{v}_2)$ onto $\mathcal{S}_1$. This is done by projecting its components $(\mathrm{v}_2^1, \mathrm{v}_2^2, \mathrm{v}_2^3)$ onto $\mathcal{S}_1$ and by expressing (x_1, y_1, z_1) as functions of (x_2, y_2, z_2), as v_2 is only defined on $\mathcal{S}_2$. This is done using (4.2). The second equation of system (4.3) is obtained in a similar manner, where the roles of v_1 and v_2 are reversed.

The functional equations system solved by the spectral functions is obtained by substituting the integral formulation (3.26) of v_1 and v_2 into (4.3), evaluating the first equation of (4.3) at $x_1 \geq 0, y_1 = 0$ and the second at $x_2 \geq 0, y_2 = 0$ and applying the Fourier transform to the result. This yields :

$$\begin{aligned} \int_0^{+\infty} e^{-ix\xi} B_1(\mathrm{v}_1)(\mathrm{x})\,\mathrm{dx} &= \frac{1}{2}\mathbf{DM}(\Sigma_1)(\xi) \\ &= \frac{1}{2}\int_{\Gamma_0} \mathbf{DM}(\xi,\zeta)\Sigma_1(\zeta)\,d\zeta \end{aligned} \tag{4.6}$$

where

$$\begin{aligned} \mathbf{DM}(\xi,\zeta) &= \frac{1}{2i\pi}\frac{1}{\xi-\zeta}\mathbf{dm}(\zeta) \\ &= \frac{1}{2i\pi}\frac{1}{\xi-\zeta}\begin{pmatrix} -1 & \frac{\zeta}{\zeta_T}(1-2\mu Q(\zeta)) & 0 \\ -\frac{\zeta}{\zeta_L}(1-2\mu Q(\zeta)) & -1 & -\frac{\tau}{\zeta_L}(1-2\mu Q(\zeta)) \\ 0 & \frac{\tau}{\zeta_T}(1-2\mu Q(\zeta)) & -1 \end{pmatrix}, \end{aligned} \tag{4.7}$$

$\zeta_*, * = L, T$ are defined by taking $\varepsilon = 0$ in (3.18) and

$$Q(\zeta) = \zeta_L\zeta_T + \zeta^2 + \tau^2 \tag{4.8}$$

The evaluation of $B_2(\mathrm{v}_2)$ at $x_1 \geq 0, y_1 = 0$ is the evaluation of $B_2(\mathrm{v}_2)$ at $x_2 = x\cos\varphi, y_2 = x\sin\varphi, x \geq 0$. The Fourier transform of the second term is therefore

$$\begin{aligned} \int_0^{+\infty} e^{-ix\xi} B_2(\mathrm{v}_2)(\mathrm{x})\,\mathrm{dx} &= \frac{1}{2}\mathbf{TM}(\Sigma_2)(\xi) \\ &= \frac{1}{2}\int_{\Gamma_0} \mathbf{TM}(\xi,\zeta)\Sigma_2(\zeta)\,d\zeta \end{aligned} \tag{4.9}$$

where

$$\mathbf{TM}(\xi,\zeta) = \frac{1}{2i\pi}\sum_{*=L,TH,TV} D_*(\xi,\zeta)\mathbf{tm}_*(\zeta, \mathrm{sgn}\ \sin\varphi), \tag{4.10}$$

$$D_*(\xi,\zeta) = \frac{1}{\xi - (\zeta\cos\varphi + \zeta_*(\zeta)|\sin\varphi|)} \tag{4.11}$$

We note ϵ =sgn sin φ, and the following matrices $\mathrm{tm}_*, * = L, TH, TV$ of rank 1 are defined :

$$\begin{cases} \mathbf{tm}_L(\zeta) = \left[\frac{\zeta}{\zeta_L}f_L\,;\ \epsilon f_L\,;\ \frac{\tau}{\zeta_L}f_L\right] \\ f_L = \begin{pmatrix} \mu[\cos(2\varphi)(2\epsilon\zeta\zeta_L) - \sin(2\varphi)(\zeta^2 - \zeta_L^2)] \\ -\lambda + 2\mu[\sin(2\varphi)(\epsilon\zeta\zeta_L) - \zeta^2\sin^2\varphi - \zeta_L^2\cos^2\varphi] \\ -2\mu\tau[\zeta\sin\varphi - \epsilon\zeta_L\cos\varphi] \end{pmatrix}, \end{cases} \tag{4.12}$$

$$\begin{cases} \mathbf{tm}_{TH}(\zeta) = [-tf_{TH}\,;\,\frac{\zeta}{\zeta_T}f_{TH}\,;\,0] \\ f_{TH} = \mu\left(1+\frac{\tau^2}{\zeta^2+\zeta_T^2}\right)\begin{pmatrix}\sin(2\varphi)(2\epsilon\zeta\zeta_T)+\cos(2\varphi)(\zeta^2-\zeta_T^2)\\ \sin(2\varphi)(\zeta^2-\zeta_T^2)-\cos(2\varphi)(2\epsilon\zeta\zeta_T)\\ \tau[\epsilon\zeta_T\sin\varphi+\zeta\cos\varphi]\end{pmatrix}\end{cases} \tag{4.13}$$

and

$$\begin{cases} \mathbf{tm}_{TV}(\zeta) = [\frac{\zeta\tau}{\zeta_T(\zeta^2+\zeta_T^2)}f_{TV}\,;\,\frac{\epsilon\tau}{\zeta^2+\zeta_T^2}f_{TV}\,;\,-\frac{1}{\zeta_T}f_{TV}] \\ f_{TV} = \mu\begin{pmatrix}\tau\cos(2\varphi)(2\epsilon\zeta\zeta_T)-\tau\sin(2\varphi)(\zeta^2-\zeta_T^2)\\ 2\tau[\sin(2\varphi)(\epsilon\zeta\zeta_T)-\zeta^2\sin^2\varphi-\zeta_T^2\cos^2\varphi]\\ \left(\tau^2-\zeta^2+\zeta_T^2\right)[\epsilon\zeta_T\cos\varphi-\zeta\sin\varphi]\end{pmatrix}\end{cases} \tag{4.14}$$

In the following, let us note for simplification:

$$\mathbf{tm}_T = \mathbf{tm}_{TH} + \mathbf{tm}_{TV} \tag{4.15}$$

It has been checked that setting $\tau = 0$ in the explicit expressions of **DM** and **TM** operators leads to the same expressions as those found in the 2D case and given by Chehade et al. [44].

Finally, the Fourier transform of the boundary conditions on the wedge faces is obtained by summing (4.6) and (4.9). The right-hand side of the system is obtained by taking the Fourier transform of $-B\mathrm{v}_\alpha^{\mathrm{inc}}|_{S_\mathrm{j}}$, j = 1, 2, where B is defined by (2.16) and the incident field is given by (2.17). The final system of functional equations solved by the spectral functions is

$$\begin{cases} \mathbf{DM}(\Sigma_1) + \mathbf{TM}(\Sigma_2) = \dfrac{W_1^\alpha}{\xi - \nu_\alpha\cos\theta_{inc}\cos\delta_{inc}} \\ \mathbf{TM}(\Sigma_1) + \mathbf{DM}(\Sigma_2) = \dfrac{W_2^\alpha}{\xi - \nu_\alpha\cos(\varphi-\theta_{inc})\cos\delta_{inc}} \end{cases} \tag{4.16}$$

where

$$W_1^L = -2\begin{pmatrix}\mu\cos^2\delta_{inc}\sin(2\theta_{inc})\\ 1-2\mu(\cos^2\theta_{inc}\cos^2\delta_{inc}+\sin^2\delta_{inc})\\ \mu\sin(2\delta_{inc})\sin(\theta_{inc})\end{pmatrix} \qquad W_2^L = -2\begin{pmatrix}\mu\cos^2\delta_{inc}\sin(2\varphi-2\theta_{inc})\\ 1-2\mu(\cos^2(\varphi-\theta_{inc})\cos^2\delta_{inc}+\sin^2\delta_{inc})\\ \mu\sin(2\delta_{inc})\sin(\varphi-\theta_{inc})\end{pmatrix}$$

$$W_1^{TV} = 2\nu_T\mu\begin{pmatrix}\frac{1}{2}\sin(2\theta_{inc})\sin(2\delta_{inc})\\ \sin(2\delta_{inc})\sin^2\theta_{inc}\\ -\sin\theta_{inc}\cos(2\delta_{inc})\end{pmatrix} \qquad W_2^{TV} = 2\nu_T\mu\begin{pmatrix}\frac{1}{2}\sin(2\varphi-2\theta_{inc})\sin(2\delta_{inc})\\ \sin(2\delta_{inc})\sin^2(\varphi-\theta_{inc})\\ -\sin(\varphi-\theta_{inc})\cos(2\delta_{inc})\end{pmatrix} \tag{4.17}$$

$$W_1^{TH} = -2\nu_T\mu\begin{pmatrix}\cos\delta_{inc}\cos(2\theta_{inc})\\ \sin(2\theta_{inc})\cos\delta_{inc}\\ \cos\theta_{inc}\sin\delta_{inc}\end{pmatrix} \qquad W_2^{TH} = 2\nu_T\mu\begin{pmatrix}\cos\delta_{inc}\cos(2\varphi-2\theta_{inc})\\ \sin(2\varphi-2\theta_{inc})\cos\delta_{inc}\\ \cos(\varphi-\theta_{inc})\sin\delta_{inc}\end{pmatrix}$$

Thanks to these functional equations, the spectral functions can be decomposed into two parts : a singular function and a regular function. The evaluation of each of these parts is described in the following.

4.2. Singular part

The first step in evaluating the spectral functions is to determine their poles and corresponding residues. This is done by a recursive procedure, using the following translation function which appears in (4.11) (for $* = L, T$) :

$$T_*(\xi = \tilde{\nu}_*\cos\theta) = \xi\cos\varphi + \zeta_*(\xi)\sin\tilde{\varphi} = \tilde{\nu}_*\cos(\theta+\tilde{\varphi}) \tag{4.18}$$

where $\tilde{\varphi}$ is defined by

$$\tilde{\varphi} = \begin{cases}\varphi & \text{if} \quad 0<\varphi<\pi \\ 2\pi-\varphi & \text{if} \quad \pi<\varphi<2\pi\end{cases} \tag{4.19}$$

This translation operator is defined on subspace Ω_*^+, represented on Fig. 5 :

$$\xi \in \Omega_*^+ = \{\xi = \tilde{\nu}_*\cos\theta,\ 0 \le \mathrm{Re}\theta < \pi - \tilde{\varphi}\} \tag{4.20}$$

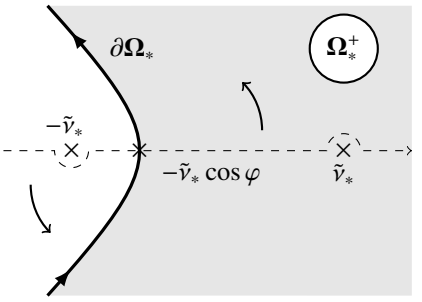

Fig. 5: Contour $\partial\Omega_*$ and domain Ω_*^+. The curved arrows show deformation of contour Γ_0 onto $\partial\Omega_*$.

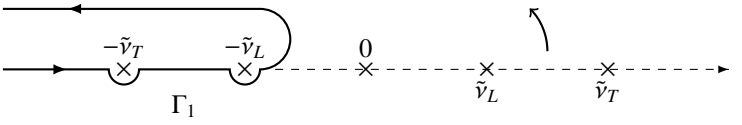

Fig. 6: Contour Γ_1 in the complex plane. The arrow shows the deformation of contour Γ_0 into Γ_1.

In order to determine the action of operator **DM** on a simple pole z, Im$z \geq 0$, contour Γ_0 in (4.6) is deformed into contour Γ_1. Contour Γ_1 is visible in Fig. 6 and Cauchy's residue theorem can then be applied for Im$z \geq 0$, Im$\xi < 0$ with $z \in \mathbb{C}\backslash(]-\infty, -\tilde{\nu}_L] \cup \{\pm\tilde{\nu}_L, \pm\tilde{\nu}_T\})$, yielding :

$$\int_{\Gamma_0} \mathbf{DM}(\xi,\zeta).\frac{1}{\zeta - z}\, d\zeta = \frac{\mathbf{dm}(z)}{\xi - z} + \mathbf{D_p}(z,\xi), \tag{4.21}$$

where

$$\mathbf{D_p}(z,\xi) = \int_{\Gamma_1} \frac{\mathbf{DM}(\xi,\zeta)}{\zeta - z}\, d\zeta \tag{4.22}$$

Similarly, in order to determine the action of operator **TM** on a simple pole z, Im$z \geq 0$, contour Γ_0 in (4.9) is deformed into contour $\partial\Omega_L$ for the L terms and $\partial\Omega_T$ for the T terms, both of which are visible in Fig. 5. Cauchy's residue theorem is applied, yielding, for Im$z \geq 0$, Im$\xi < 0$ with $z \in \mathbb{C}\backslash(]-\infty, -\tilde{\nu}_L] \cup \{\pm\tilde{\nu}_L, \pm\tilde{\nu}_T\})$:

$$\int_{\Gamma_0} \mathbf{TM}(\xi,\zeta).\frac{1}{\zeta - z}\, d\zeta = \sum_{*=L,T} \frac{\mathbf{tm}_*(z)}{\xi - T_*(z)} \mathbf{1}_{\Omega_*}(z) + \mathbf{T_p}(z,\xi) \tag{4.23}$$

where $\mathbf{1}_{\Omega_*}(z) = 1$ if $z \in \Omega_*$ and $\mathbf{1}_{\Omega_*}(z) = 0$ elsewhere and

$$\mathbf{T_p}(z,\xi) = \frac{1}{2i\pi} \sum_{*=L,T} \int_{\partial\Omega_*} D_*(\xi,\zeta).\frac{\mathbf{tm}_*(\zeta)}{\zeta - z}\, d\zeta \tag{4.24}$$

It is important to note that in all the aforementioned contour deformations, no branch points $\pm\tilde{\nu}_L$ or $\pm\tilde{\nu}_T$ of the integrands are crossed. Therefore, it is assumed that Croisille and Lebeau's [41] proof that $\mathbf{D_p}(z,\cdot)$ and $\mathbf{T_p}(z,\cdot)$ belong to a special class of functions $\mathcal{H}^3$ can be adapted to the 3D case. It will therefore be assumed that $\mathbf{D_p}(z,\cdot) \in \mathcal{H}^3$ and $\mathbf{T_p}(z,\cdot) \in \mathcal{H}^3$ where $\mathcal{H}$ is defined hereafter

Def. 4.1. *H^+ is the space of functions f which are analytical in $\{z \in \mathbb{C},\ Imz < 0\}$ and verify :*

$$\sup_{c>0} \int_{-\infty}^{+\infty} |f(x - ic)|^2\, dx < +\infty \tag{4.25}$$

Def. 4.2. *$\mathcal{H}$ is the space of the functions f analytical in $\mathbb{C}\backslash]-\infty, -\tilde{\nu}_L]$ such that $\forall\varepsilon \in]0, \pi[$, $f(e^{i\varepsilon}\cdot) \in H^+$.*

The poles and corresponding residues of the spectral functions are extracted by recursively injecting decompositions (4.21) and (4.23) into the system of functional equations (4.16). The procedure is analogous to the one detailed in [44] and will not be repeated here. In the end, we have, for Im$\xi < 0$

$$\Sigma_j(\xi) = Y_j(\xi) + X_j(\xi) \tag{4.26}$$

where

$$Y_j(\xi) = \sum_k \sum_{*=L,T} \frac{V_{j,*}^{(k)}}{\xi - Z_{j,*}^{(k)}}, \tag{4.27}$$

with

$$\begin{array}{cc} Z_1^{(0)} = \nu_\alpha \cos\theta_{inc} \cos\delta_{inc}, & Z_2^{(0)} = \nu_\alpha \cos(\varphi - \theta_{inc}) \cos\delta_{inc} \\ Z_{j,L}^{(k+1)} = T_L(Z_{3-j,*}^{(k)}) & Z_{j,T}^{(k+1)} = T_T(Z_{3-j,*}^{(k)}) \end{array} \tag{4.28}$$

and

$$\begin{array}{c} V_j^{(0)} = \mathbf{dm}^{-1}(Z_j^{(0)}).W_j^\alpha \\ V_{j,L}^{(k+1)} = -\mathbf{dm}^{-1}(Z_{j,*}^{(k+1)}).\mathbf{tm}_L(Z_{3-j,*}^{(k)}).V_{3-j,*}^{(k)}.\mathbf{1}_{\Omega_L}(Z_{3-j,*}^{(k)}) \\ V_{j,T}^{(k+1)} = -\mathbf{dm}^{-1}(Z_{j,*}^{(k+1)}).\mathbf{tm}_T(Z_{3-j,*}^{(k)}).V_{3-j,*}^{(k)}.\mathbf{1}_{\Omega_T}(Z_{3-j,*}^{(k)}) \end{array} \tag{4.29}$$

where W_j^α is given by (4.17). The recursive procedure stops when no more poles can be found by deforming contour Γ_0 into $\partial\Omega_L$ or $\partial\Omega_T$. In the 2D case, Croisille and Lebeau [41] have shown that this defines a finite number of poles. The sequence of poles generated in the 3D case being similar to the ones generated in the 2D case (parameters ν_L and ν_T in the 2D case are replaced by parameters $\tilde{\nu}_L$ and $\tilde{\nu}_T$), their demonstration is still valid here. Physically, this means that any incident ray leaves the wedge after a finite number of reflections. We have thus extracted all the poles from the spectral functions and have computed them analytically using (4.28), along with their corresponding residues (4.29) to completely determine the singular part (4.27) of the spectral functions.

4.3. Regular Part

The singular parts Y_j of the spectral functions having been determined, two new regular functions X_1 and X_2 are defined by (4.26). In the following, a numerical approximation method for X_j is proposed. In order to do so, a system of functional equations solved by X_1, X_2 is derived by subtracting vector

$$\begin{pmatrix} \mathbf{DM}(Y_1) + \mathbf{TM}(Y_2) \\ \mathbf{TM}(Y_1) + \mathbf{DM}(Y_2) \end{pmatrix}, \tag{4.30}$$

from both sides of (4.16), where Y_1 and Y_2 are given by equations (4.27) to (4.29) :

$$\begin{cases} \mathbf{DM}(X_1)(\xi) + \mathbf{TM}(X_2)(\xi) = u_1(\xi) \\ \mathbf{TM}(X_1)(\xi) + \mathbf{DM}(X_2)(\xi) = u_2(\xi) \end{cases}, \tag{4.31}$$

with, for $j = 1, 2$

$$u_j(\xi) = -\sum_k \sum_{*=L,T} \left[\mathbf{D_p}(Z_{j,*}^{(k)}, \xi).V_{j,*}^{(k)} + \mathbf{T_p}(Z_{3-j,*}^{(k)}, \xi).V_{3-j,*}^{(k)} \right] \tag{4.32}$$

It is assumed that Kamotski and Lebeau's [43] proof that this system has a unique solution can be adapted to the 3D case, meaning that system (4.31) has a unique solution (X_1, X_2) in $\mathcal{H}^3$ where $\mathcal{H}$ is defined by Def. 4.2. A numerical approximation of the regular parts X_j will be computed using Galerkin's collocation method.

The functional space $\mathcal{H}$ is approached by the finite-dimension subspace generated by basis functions $(\varphi_k)_{1\leq k\leq N}$ defined as:

$$\varphi_k(\xi) = \sqrt{\frac{a_k}{\pi}} \frac{1}{\xi + a_k}, \qquad (a_k)_{1\leq k\leq N} \in ([\tilde{\nu}_L, +\infty[)^N \tag{4.33}$$

For a point $a_k \in [\tilde{\nu}_L, +\infty[$, the corresponding Galerkin function φ_k will have a pole at $-a_k \in]-\infty, -\tilde{\nu}_L]$. The basis $(\varphi_k)_{1\leq k\leq N}$ therefore generates a subspace of functions analytical in $\mathbb{C}\backslash]-\infty, -\tilde{\nu}_L]$.

Functions X_j are approximated in the adapted finite dimension subspace by :

$$X_j(\xi) \approx \sum_{k=1}^{N} \tilde{X}_j^k \varphi_k(\xi), \quad \tilde{X}_j^k \in \mathbb{C}^3 \tag{4.34}$$

Galerkin approximation (4.34) is substituted into (4.31) and the variable change $\zeta = iy$ is applied in the resulting system. This system is then evaluated at collocation points $\xi = b_1, ..., b_N$ (in practice, these collocation points are

chosen to be located right below points a_k in the complex plane, see (5.1)). This leads to a linear system of equations which can be written in matrix form :

$$\begin{pmatrix} \mathbb{D} & \mathbb{T} \\ \mathbb{T} & \mathbb{D} \end{pmatrix} \begin{pmatrix} \mathbb{X}_1 \\ \mathbb{X}_2 \end{pmatrix} = \begin{pmatrix} \mathbb{U}_1 \\ \mathbb{U}_2 \end{pmatrix}, \tag{4.35}$$

where matrices $\mathbb{D}$ and $\mathbb{T}$ are defined by 3×3 blocks:

$$\begin{aligned} \mathbb{D}_{lk} &= \int_{-\infty}^{+\infty} \mathbf{DM}(b_l, iy) e_{a_k}(y)\, dy = \frac{1}{2i\pi} \int_{-\infty}^{+\infty} \frac{\mathbf{dm}}{b_l - iy} \sqrt{\frac{a_k}{\pi}} \frac{1}{y - ia_k}\, dy \\ &= -\frac{\sqrt{a_k}}{2\pi\sqrt{\pi}} \begin{pmatrix} \mathcal{D}_1(a_k, b_l) & \mathcal{D}_2^T(a_k, b_l) & 0 \\ -\mathcal{D}_2^L(a_k, b_l) & \mathcal{D}_1(a_k, b_l) & -\mathcal{D}_3^L(a_k, b_l) \\ 0 & \mathcal{D}_3^T(a_k, b_l) & \mathcal{D}_1(a_k, b_l) \end{pmatrix} = \frac{\sqrt{a_k}}{2\pi\sqrt{\pi}} \mathbb{D}(a_k, b_l) \end{aligned} \tag{4.36}$$

where functions e_{a_k} are defined by

$$e_{a_k}(y) = \sqrt{\frac{a_k}{\pi}} \frac{1}{y - ia_k},\ 1 \le k \le N. \tag{4.37}$$

The explicit expressions of coefficients of matrix $\mathbb{D}(a, b)$ and their values are computed in Appendix A.

The other matrices involved are, for $1 \le l, k \le N$

$$\begin{aligned} \mathbb{T}_{lk} &= \int_{-\infty}^{+\infty} \mathbf{TM}(b_l, iy) e_{a_k}(y)\, dy = \frac{1}{2i\pi} \int_{-\infty}^{+\infty} \sum_{*=L,T} \frac{\mathbf{tm}_*(iy, \operatorname{sgn}\sin\varphi)}{b_l - T_*(iy)} \sqrt{\frac{a_k}{\pi}} \frac{1}{y - ia_k}\, dy \\ &= \frac{1}{2i\pi} \sqrt{\frac{a_k}{\pi}} \sum_{*=L,T} \int_{-\infty}^{+\infty} \frac{\mathbf{tm}_*(iy, \epsilon)}{[b_l - (iy\cos\varphi + \zeta_*(iy)|\sin\varphi|)](y - ia_k)}\, dy, \end{aligned} \tag{4.38}$$

where $\epsilon = \operatorname{sgn}(\sin\varphi)$. Let us define

$$\mathbb{T}_{lk} = \frac{1}{2i\pi} \sqrt{\frac{a_k}{\pi}} \sum_{*=L,TH,TV} \begin{pmatrix} \mathcal{T}_1^*(a_k, b_l) & \mathcal{T}_2^*(a_k, b_l) & \mathcal{T}_3^*(a_k, b_l) \\ \mathcal{T}_4^*(a_k, b_l) & \mathcal{T}_5^*(a_k, b_l) & \mathcal{T}_6^*(a_k, b_l) \\ \mathcal{T}_7^*(a_k, b_l) & \mathcal{T}_8^*(a_k, b_l) & \mathcal{T}_9^*(a_k, b_l) \end{pmatrix} = \frac{1}{2i\pi} \sqrt{\frac{a_k}{\pi}} \mathbb{T}(a_k, b_l) \tag{4.39}$$

The explicit expressions of operators $\mathcal{T}_i^*$, $1 \le i \le 9, * = L, TH, TV$ and their values are computed in Appendix B.

Finally:

$$\mathbb{X}_j = \begin{pmatrix} \tilde{X}_j^1 \\ \vdots \\ \tilde{X}_j^{2N} \end{pmatrix} \qquad \mathbb{U}_j = \begin{pmatrix} u_j(b_1) \\ \vdots \\ u_j(b_{2N}) \end{pmatrix} \tag{4.40}$$

where $u_j(\xi)$ is given by (4.32). Applying variable change $\zeta = iy$ to the definition of D_p given by (4.21) and substituting (4.36) in the result gives

$$D_p(z, \xi) = \frac{1}{2\pi} \mathbb{D}(-z, \xi) - \frac{\mathbf{dm}(z)}{\xi - z} \tag{4.41}$$

Similarly, applying variable change $\zeta = iy$ to (4.23) and substituting (4.39) in the result yields

$$T_p(z, \xi) = \frac{1}{2i\pi} \mathbb{T}(-z, \xi) - \sum_{*=L,T} \frac{\mathbf{tm}_*(z, \epsilon)}{b - T_*(z)} \mathbf{1}_{\Omega_*}(z) \tag{4.42}$$

Equations (4.41) and (4.42) are substituted into (4.32). The singular terms cancel each other, except those of the initial poles $Z_j^{(0)}$, and the remaining terms are :

$$u_j(\xi) = -\frac{1}{2i\pi} \sum_k \sum_{*=L,T} \left(i\mathbb{D}(-Z_{j,*}^{(k)}, \xi).V_{j,*}^{(k)} + \mathbb{T}(-Z_{3-j,*}^{(k)}, \xi).V_{3-j,*}^{(k)} \right) + \frac{W_j^\alpha}{\xi - Z_j^{(0)}} \tag{4.43}$$

Using these results, the linear system (4.35) is implemented and solved numerically using the C++ library Eigen, and an evaluation of the regular part of the spectral functions is obtained. However, for values of ξ lying in certain parts of the complex plane, this evaluation is not sufficiently accurate. The technique used to solve this problem is called the propagation of the solution.

4.4. Propagation of the solution

The method called propagation of the solution is used to propagate the accuracy of the numerical approximation of the regular functions X_1 and X_2 from parts of the complex plane where they are evaluated accurately to parts of the complex plane where they are not. The validity domains in the complex plane will be detailed hereafter.

The first step of this procedure is to deform contour Γ_0 (visible in Fig. 3) in operator **DM** into contour Γ_2 in functional system (4.31). Contour Γ_2 is visible on Fig. 7. During this deformation, the half-plane $\mathrm{Im}\xi < 0$ is crossed. The pole $\zeta = \xi$ is crossed during this contour deformation when $\mathrm{Im}\xi < 0$. Its contribution is given by Cauchy's residue formula :

$$\int_{\Gamma_0} \mathbf{DM}(\xi,\zeta)X_j(\zeta)\,d\zeta = \int_{\Gamma_2} \mathbf{DM}(\xi,\zeta)X_j(\zeta)\,d\zeta + \mathbf{dm}(\xi).X_j(\xi) \tag{4.44}$$

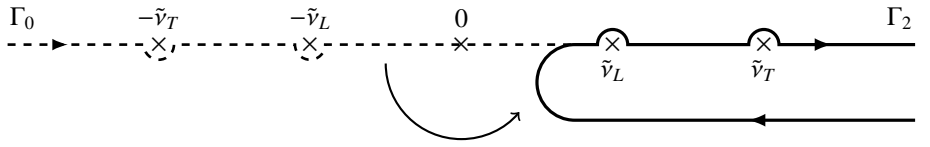

Fig. 7: Integration contour Γ_2. The curved arrow indicates the contour deformation from Γ_0 to Γ_2.

The next step is to define the inverse translation operator $T_*^{-1} : \Omega_*^- \to \mathbb{C}, * = L, T$:

$$T_*^{-1}(\xi = \nu_* \cos\theta) = \xi\cos\tilde{\varphi} - \zeta_*(\xi)\sin\tilde{\varphi} = \nu_*\cos(\theta - \tilde{\varphi}). \tag{4.45}$$

$\cos\theta$ is well defined for $0 \leq \mathrm{Re}\theta \leq \pi$, therefore this operator is defined on subspace Ω_*^-, visible on Fig. 8 and defined as

$$\Omega_*^- = \{\xi \in \mathbb{C},\ \xi = \tilde{\nu}_* \cos\theta, \tilde{\varphi} \leq \mathrm{Re}(\theta) \leq \pi\} \tag{4.46}$$

Using these definitions, contour Γ_0 in operator **TM** is deformed into contour $\partial\Omega_*^-$, visible on Fig. 8. The contours are represented in Fig. 8, and the deformation from Γ_0 to $\partial\Omega_*^-$ (represented by the arrows on the figure) only spans the bottom half of domain Ω_*^-. The poles ζ of the integrand are $\zeta = T_*^{-1}(\xi), \mathrm{Im}\xi < 0$. These poles are crossed if and only if $\xi \in \Omega_*^-$ and $\mathrm{Im}\xi < 0$, where domain Ω_*^- is represented in grey on Fig. 8. Their contribution is determined thanks to Cauchy's residue theorem :

$$\int_{\Gamma_0} \mathbf{TM}(\xi,\zeta)X_j(\zeta)\,d\zeta = \sum_{*=L,T} \int_{\partial\Omega_*^-} \frac{\mathbf{tm}_*(\zeta)}{\xi - T_*(\zeta)}.X_j(\zeta)\,d\zeta + \mathbf{M}_*(\xi).X_j(T_*^{-1}(\xi))\mathbf{1}_{\Omega_*^-}(\xi), \tag{4.47}$$

where $\mathbf{1}_{\Omega_*^-}(\xi) = 1$ when $\xi \in \Omega_*^-$ and $\mathrm{Im}\xi < 0$ and $\mathbf{1}_{\Omega_*^-}(\xi) = 0$ elsewhere and

$$\mathbf{M}_*(\xi = \tilde{\nu}_*\cos\theta) = -\frac{\sin(\theta - \tilde{\varphi})}{\sin\theta}\mathbf{tm}_*(T_*^{-1}(\xi)) \tag{4.48}$$

The recursive system of functional equations solved by the regular part is obtained by substituting (4.44) and (4.47) into (4.31):

$$\begin{cases} X_1(\xi) = g_1(\xi) - \mathbf{dm}^{-1}(\xi).\sum\limits_{*=L,T} \mathbf{M}_*(\xi).X_2(T_*^{-1}(\xi))\mathbf{1}_{\Omega_*^-}(\xi) \\ X_2(\xi) = g_2(\xi) - \mathbf{dm}^{-1}(\xi).\sum\limits_{*=L,T} \mathbf{M}_*(\xi).X_1(T_*^{-1}(\xi))\mathbf{1}_{\Omega_*^-}(\xi) \end{cases}, \tag{4.49}$$

where, for $j = 1, 2$

$$g_j(\xi) = \mathbf{dm}^{-1}(\xi)\left(u_j(\xi) - \int_{\Gamma_2} \mathbf{DM}(\xi,\zeta)X_j(\zeta)\,d\zeta - \int_{\partial\Omega_*^-} \mathbf{TM}(\xi,\zeta)X_{3-j}(\zeta)\,d\zeta\right) \tag{4.50}$$

System (4.49) is called the recursive system because it uses the value of the regular function X_2 at points $T_*^{-1}(\xi)$, where the numerical approximation for the regular part may be valid, to compute the value of X_1 at the point ξ where the approximation is not valid (and vice-versa). If the translation from ξ to $T_*^{-1}(\xi)$ is not sufficient to reach the domain $\mathbb{C}\backslash\Omega_*^-$ where the approximation is valid, then the use of the formula is repeated as many times as necessary until

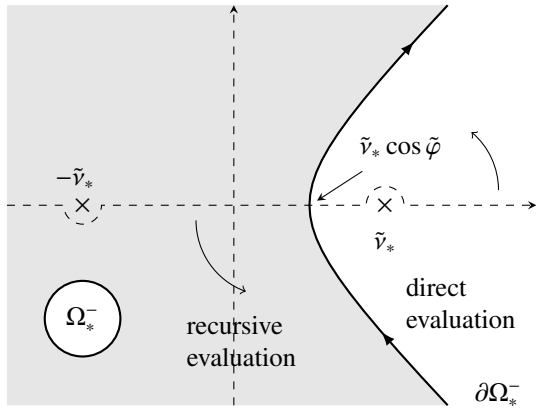

Fig. 8: Domain Ω_*^- and contour $\partial\Omega_*^-$. The arrows show the deformation from contour Γ_0 to contour $\partial\Omega_*^-$.

domain $\mathbb{C}\backslash\Omega_*^-$ is reached. In order to apply this new recursive system to evaluate the spectral functions in the domain $W = \{\mathrm{Im}(\xi) < 0, \xi \notin \Omega_*^-\}$, functions g_j must be evaluated numerically.

Each of the integrals appearing in the definition of g_j are evaluated separately using the approximation of the regular part (4.34) for the computation of terms $X_j(\zeta)$ and $X_{3-j}(\zeta)$.

Substituting (4.36) into (4.44) yields :

$$\int_{\Gamma_2} \mathbf{DM}(\xi,\zeta)\varphi_k(\zeta)\,d\zeta = \int_{\Gamma_0} \mathbf{DM}(\xi,\zeta)\varphi_k(\zeta)\,d\zeta - \mathbf{dm}(\xi).\varphi_k(\xi) = \frac{1}{2\pi}\sqrt{\frac{a_k}{\pi}}\mathbb{D}(a_k,\xi) - \mathbf{dm}(\xi).\varphi_k(\xi) \tag{4.51}$$

and substituting (4.39) into (4.47) yields:

$$\begin{aligned}\int_{\partial\Omega_*^-} \mathbf{TM}(\xi,\zeta)\varphi_k(\zeta)\,d\zeta &= \int_{\Gamma_0} \mathbf{TM}(\xi,\zeta)\varphi_k(\zeta)\,d\zeta - \sum_{*=L,T} \mathbf{M}_*(\xi).\varphi_k(T_*^{-1}(\xi)) \\ &= \frac{1}{2i\pi}\sqrt{\frac{a_k}{\pi}}\mathbb{T}(a_k,\xi) - \sum_{*=L,T} \mathbf{M}_*(\xi).\varphi_k(T_*^{-1}(\xi))\mathbf{1}_{\Omega_*^-}(\xi)\end{aligned} \tag{4.52}$$

Finally, (4.51) and (4.52) can be injected into (4.50) :

$$\mathbf{dm}(\xi).g_j(\xi) = u_j(\xi) - \sum_{k=1}^{2N} \sqrt{\frac{a_k}{\pi}}\left(\mathbb{ND}(a_k,\xi).\tilde{X}_j^k + \mathbb{NT}(a_k,\xi).\tilde{X}_{3-j}^k\right), \tag{4.53}$$

where

$$\mathbb{ND}(a,b) = \frac{1}{2\pi}\mathbb{D}(a,b) - \frac{\mathbf{dm}(b)}{a+b} \tag{4.54}$$

and

$$\mathbb{NT}(a,b) = \frac{1}{2i\pi}\mathbb{T}(a,b) - \sum_{*=L,T} \frac{\mathbf{M}_*(b)}{T_*^{-1}(b)+a}. \tag{4.55}$$

Using system (4.49), the value of the regular part of the spectral functions in domain Ω_*^-, visible Fig. 8, is calculated with respect to its value in the domain $\xi \notin \Omega_*^-$, where the numerical approximation (4.34) is valid. To do so, functions g_j, $j = 1, 2$ are evaluated numerically using (4.53). The accuracy of the numerical evaluation in domain $\xi \notin \Omega_*^-$ is therefore propagated to domain Ω_*^-.

This concludes the semi-analytical computation of the spectral functions. The L, TH and TV diffraction coefficients can now be computed using (3.37). Numerical testing is presented in the following.

5. Numerical Tests

The spectral functions are evaluated numerically using the semi-analytical scheme described in the previous sections. This is achieved by, first, computing the poles and residues of the spectral functions analytically using the

recursive algorithm described in subsection 4.2. Then, the regular parts of the spectral functions are approached numerically by solving (4.31) thanks to the Galerkin collocation method described in subsection 4.3. In the case where $\tilde{\nu}_L \in \mathbb{R}$, the Galerkin parameters are set to:

$$a_k = 1.001 + 0.05e^{k\frac{\log 10}{4}} - 1, \qquad b_k = a_k - 0.1i, \qquad 1 \leq k \leq 20 \tag{5.1}$$

Finally, the solution is rendered accurate in the entire complex domain by applying the recursive procedure called the propagation of the solution described in subsection 4.4.

Following these steps, the diffraction coefficients have been computed using (3.37) and tested numerically.

5.1. Comparison to the 2D code

The first test on the 3D code is to check that when $\delta_\alpha = 0$, the results obtained using the 3D code are the same as those obtained using the 2D code presented and validated numerically in [44] and experimentally by Chehade in her thesis [45], using the measurements made by Chapman et al. [40]. This has been checked for the theoretical computations and must also be verified numerically.

The spectral functions are evaluated at $\xi = \tilde{\nu}_L \cos\theta - i10^{-6}$ (a small negative imaginary part is added to ensure Im $\xi < 0$) every $0,5^o$ for $0 \leq \theta \leq \varphi$ and at $\delta_\alpha = 0^o$, using the 3D code. The L and TH diffraction coefficients are computed using (3.37), for an elastic wave propagating in a steel wedge ($c_L = 5700m.s^{-1}$, $c_T = 3200m.s^{-1}$). For the 3D problem, TH waves defined by (2.4) correspond to the T waves of the 2D problem. The results are compared to the diffraction coefficients obtained using the 2D elastic code presented in [44].

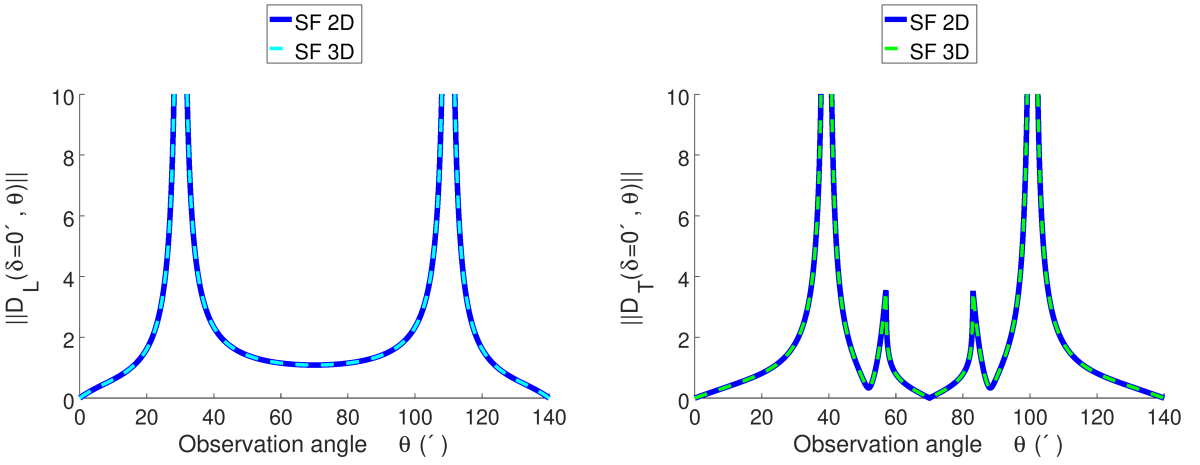

(a) Diffracted and incident L waves.

(b) Diffracted T wave and incident L wave.

Fig. 9: Diffraction coefficients for $\varphi = 140^o, \theta_{inc} = 70^o$

Figs. 9 and 10 show the absolute value of the diffraction coefficients obtained using the 2D and 3D codes for a wedge of angle $\varphi = 140^o$ illuminated by an L wave incident with an angle $\theta_{inc} = 70^o$ and for a wedge of angle $\varphi = 250^o$ illuminated by a T wave incident with an angle $\theta_{inc} = 65^o$.

In Figs. 9a-10a and Figs. 9b-10b, representing the L and T diffraction coefficients respectively, the thick blue line represents the results obtained using the 2D code and the dashed lines (cyan and green respectively) represent the results obtained using the 3D code.

In all of these figures (and in all other tested configurations) the 2D and 3D plots are perfectly overlapping. When $\delta_\alpha = 0^o$, the 3D code yields exactly the same results as the 2D code, which is in accord with the theoretical formulations. This validates the computation of the "2D terms" (meaning the terms that are not canceled by setting $\delta_\alpha = 0^o$) of the 3D code. The following numerical test, comparison of the 3D elastic code to Sommerfeld's analytical expression for an incident acoustic wave, validates a different set of terms (the ones that are purely 3D and longitudinal) computed by the spectral functions method.

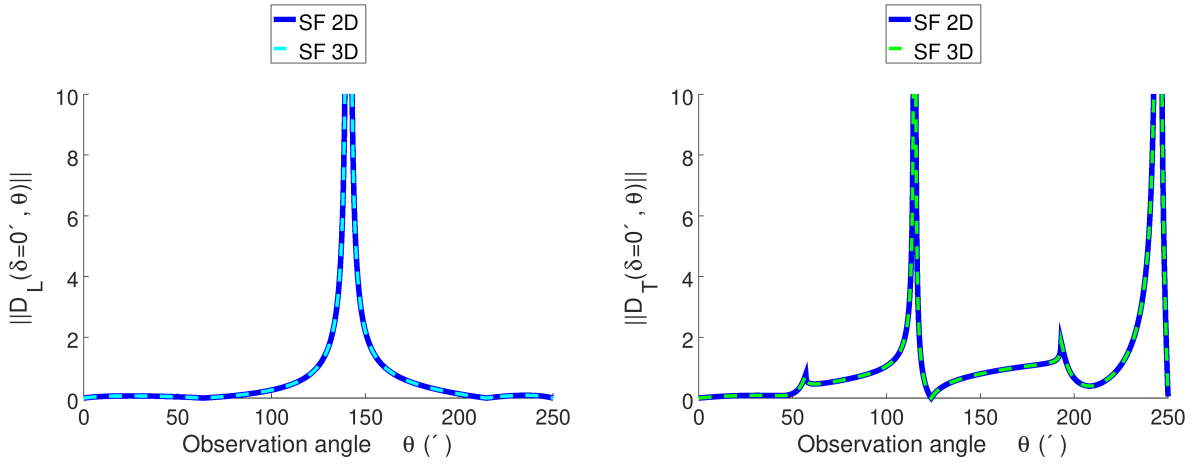

(a) Diffracted L wave and incident T wave.

(b) Diffracted and incident T waves.

Fig. 10: Diffraction coefficients for $\varphi = 250^o, \theta_{inc} = 65^o$

5.2. *Acoustic limit*

Sommerfeld [1] provides an analytical expression for the diffracted field in the case of an acoustic wave incident on a wedge with Dirichlet or Neumann boundaries. This expression is valid for 3D incidences, and the corresponding GTD field is provided by Keller [14]. In the case of a wedge with Dirichlet boundaries, we have :

$$\mathrm{v}^{ac,diff}(r,\theta) = D^{Dir}(\theta)\frac{e^{-ik_0 r}}{\sqrt{k_0 r\cos\delta_\alpha}} \tag{5.2}$$

where $v^{ac,diff}$ is the acoustic diffracted field, k_0 is the acoustic wave number and D^{Dir} is the diffraction coefficient:

$$D^{Dir}(\theta) = \frac{e^{-i\frac{\pi}{4}}}{2\mathcal{N}\sqrt{2\pi}}\left[\cot\left(\frac{\pi+(\theta+\theta_{inc})}{2\mathcal{N}}\right)+\cot\left(\frac{\pi-(\theta+\theta_{inc})}{2\mathcal{N}}\right)-\cot\left(\frac{\pi+(\theta-\theta_{inc})}{2\mathcal{N}}\right)-\cot\left(\frac{\pi-(\theta-\theta_{inc})}{2\mathcal{N}}\right)\right], \tag{5.3}$$

where $\mathcal{N} = \varphi/\pi$.

Note that for an acoustic wave, the diffraction coefficient does not depend on the incident skew angle δ_α. The dependency of the diffracted field with respect to this parameter is fully contained in the term $(k_0 r\cos\delta_\alpha)^{-1/2}$ in (5.2).

The case of an acoustic wave incident on a wedge with Dirichlet boundary conditions can be mimicked using the elastic code. By setting $c_L = 1$ and $c_T \to 0$ and considering incident L waves, the L diffraction coefficient should behave like the diffraction coefficient of an acoustic wave.

In the 3D elastic code, the wave velocities are set to $c_L = 1m.s^{-1}$ and $c_T = 10^{-7}m.s^{-1}$ and the incident wave is longitudinal. The spectral functions are evaluated at $\xi = \tilde{\nu}_L\cos\theta - i10^{-6}$ every $0,5^o$ for $0 \le \theta \le \varphi$ and for $-90^o \le \delta_\alpha \le 90^o$ and the L diffraction coefficient is deduced using (3.37).

The diffraction coefficients are computed for various incident skew angles δ_α to check that the SF diffraction coefficient is independent of this parameter, as it should be in the acoustic case. The diffraction coefficients can therefore be plotted for a single skew angle, without loss of generality. The results are compared to the analytical expression of the Sommerfeld diffraction coefficients for a wedge with Dirichlet boundary conditions.

Figs. 11 and 12 respectively show the absolute value and the angular phase of the diffraction coefficient, plotted for $\delta_\alpha = 0^o$ for a wave incident with an angle $\theta_\alpha = 40^o$ on a wedge of angle $\varphi = 160^o$ (see Figs. 11a and 12a) and for a wave incident with an angle $\theta_\alpha = 240^o$ on a wedge of angle $\varphi = 280^o$ (see Figs. 11b and 12b).

In all four figures, the thick blue line is the solution computed using Sommerfeld's analytical expression and the dashed red line is the result obtained using acoustic limit of the 3D SF code.

Both lines are perfectly overlapping, except for some discrepancies in the angular phase, for observation directions near the wedge faces.

The "acoustic limit" of the 3D elastic code is thus validated for wedge angles lower and higher than π. This shows that the terms appearing in the evaluation of the spectral functions that depend on $\tilde{\nu}_T$ tend to 0 when transversal wave velocity tends to 0 (as they should) and that the terms that depend on $\tilde{\nu}_L$ are computed correctly.

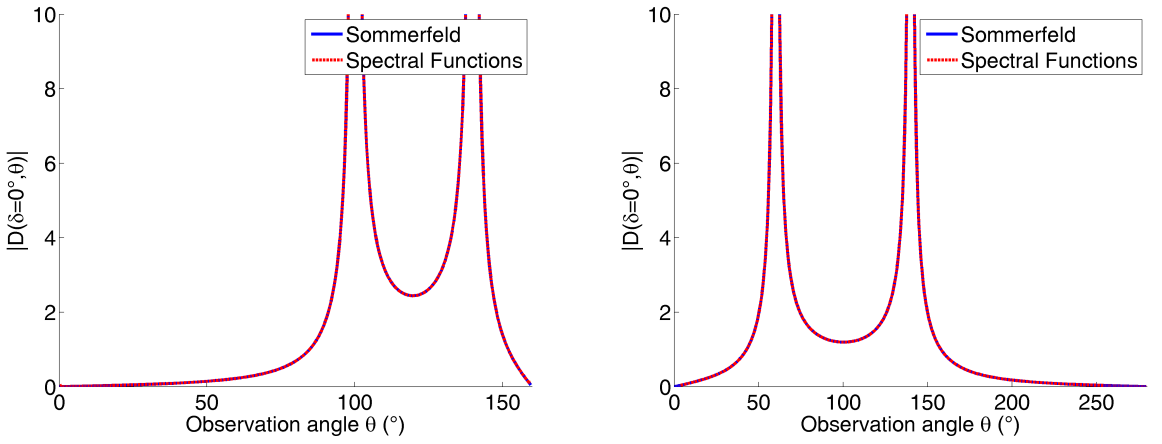

(a) $\varphi = 160^o,\ \theta_{inc} = 40^o$ (b) $\varphi = 280^o,\ \theta_{inc} = 240^o$

Fig. 11: Absolute value of the diffraction coefficient computed with the spectral functions and with the Sommerfeld method for $\delta_{inc} = 0^o$.

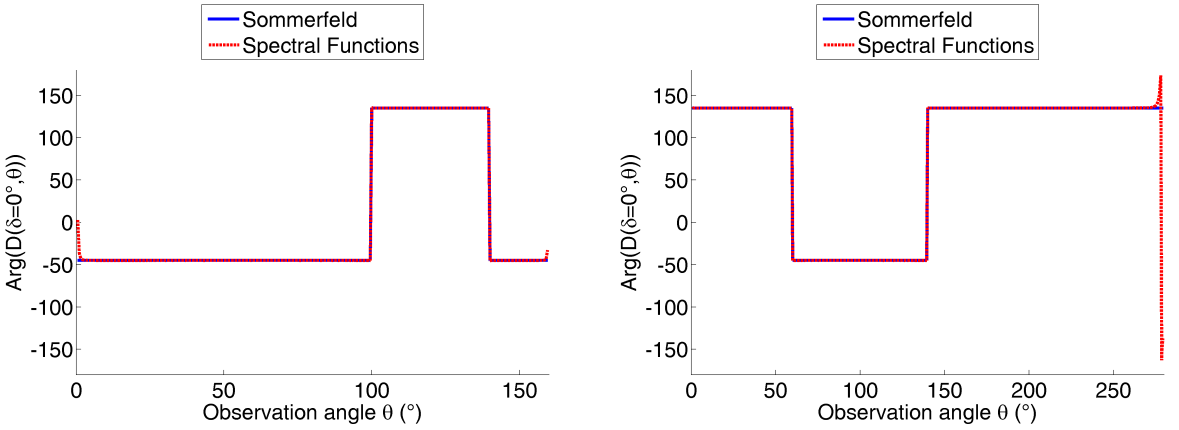

(a) $\varphi = 160^o,\ \theta_{inc} = 40^o$ (b) $\varphi = 280^o,\ \theta_{inc} = 240^o$

Fig. 12: Angular phase of the diffraction coefficient computed with the spectral functions and with the Sommerfeld method for $\delta_{inc} = 0^o$.

5.3. Verification of the regular part for an infinite plane

In the case where $\varphi = \pi$, the wedge degenerates into an infinite plane and there is no edge diffracted wave. The regular part of the spectral functions, which is determined by system (4.35) and is the part of the solution corresponding to the diffraction phenomena, vanishes and we should have, for $j = 1, 2$:

$$\|\mathbb{U}_j\| = 0 \tag{5.4}$$

where $\mathbb{U}_j$ is the right-hand side of system (4.35) and is given by (4.40). Verifying that this is the case provides a check on the lengthy computations of the explicit expressions of operators $\mathbb{D}(\cdot,\cdot)$ and $\mathbb{T}(\cdot,\cdot)$. According to (4.40), the value of $\|\mathbb{U}_j\|$ does not depend on the observation angle θ, therefore in our tests, only the skew incidence angle δ_α varies.

Fig. 13 shows $\|\mathbb{U}_j\|$, $j = 1, 2$ for incident L (Fig. 13a), TH (Fig. 13b) and TV (Fig. 13c) waves with an angle $\theta_{inc} = 50^o$ on an infinite plane. In the case of incident T waves, the results are only plotted for $\delta_\alpha < \delta_c \approx 34^o$ in the case of a steel wedge. The thick blue line represents $\|\mathbb{U}_1\|$ and the dashed red line represents $\|\mathbb{U}_2\|$. As expected, $\|\mathbb{U}_1\|$ and $\|\mathbb{U}_2\|$ are very small, of the order of the numerical computation error. This numerical computation error can be estimated by evaluating the resolution error of linear system (4.35) for various test cases.

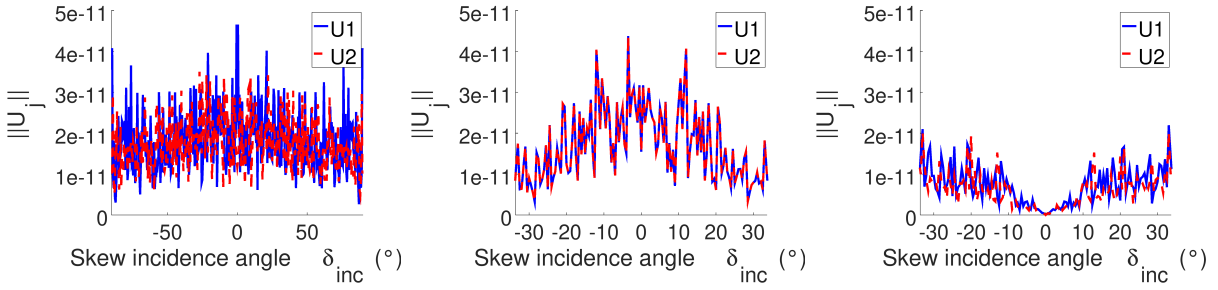

(a) Incident L wave (b) Incident TH wave (c) Incident TV wave

Fig. 13: $\|\mathbb{U}_j\|$, $j = 1, 2$ for $\varphi = 180^o$ and $\theta_{inc} = 50^o$

5.4. Example of 3D diffraction coefficients

The 3D spectral functions method has been validated in the special case of a 2D incidence, in the case of an incident acoustic wave and in the case where the wedge is degenerated into an infinite half-plane. Let us now consider the results obtained in a more general case.

Figs. 14 and 15 show the absolute value of the diffraction coefficients obtained using the SF code. The L, TH and TV diffraction coefficients are computed using (3.37) for two steel wedges ($c_L = 5700m.s^{-1}$ and $c_T = 3200m.s^{-1}$) of angles $\varphi = 150^o$ and $\varphi = 200^o$ illuminated by an incident L wave with an angle $\theta_{inc} = 65^o$ and $\theta_{inc} = 40^o$ respectively. The spectral functions are evaluated at $\xi = \tilde{\nu}_\beta \cos\theta - i10^{-6}$ every $0,5^o$ for $0 \leq \theta \leq \varphi$ and for $-90^o \leq \delta_\alpha \leq 90^o$. In both figures, the horizontal axis corresponds to the observation angle θ, the vertical axis corresponds to the incident skew angle δ_α and the magnitude of the diffraction coefficient is represented in color in the (θ, δ_α) plane. Figs. 14a and 15a show the L diffraction coefficients, Figs. 14b and 15b show the TH diffraction coefficient and Figs. 14c and 15c show the TV diffraction coefficient (note that this coefficient is cancelled in the 2D case corresponding to $\delta_\alpha = 0^o$).

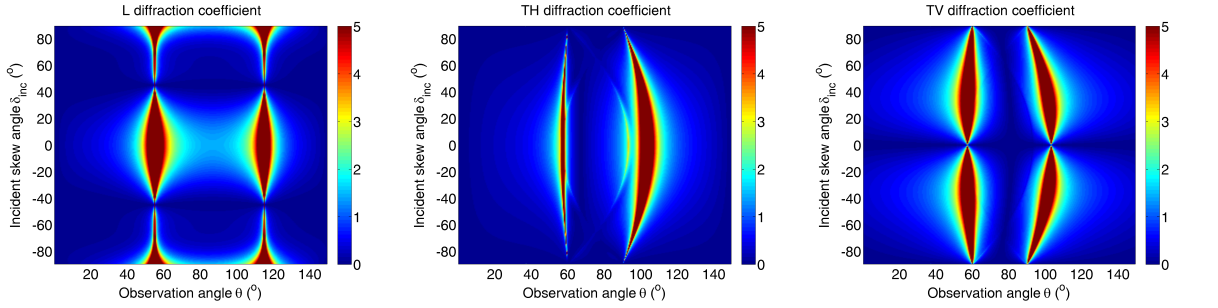

(a) Diffracted L wave (b) Diffracted TH wave (c) Diffracted TV wave

Fig. 14: Absolute value of the diffraction coefficient computed for an incident L wave on a wedge of angle $\varphi = 150^o$ with $\theta_{inc} = 65^o$

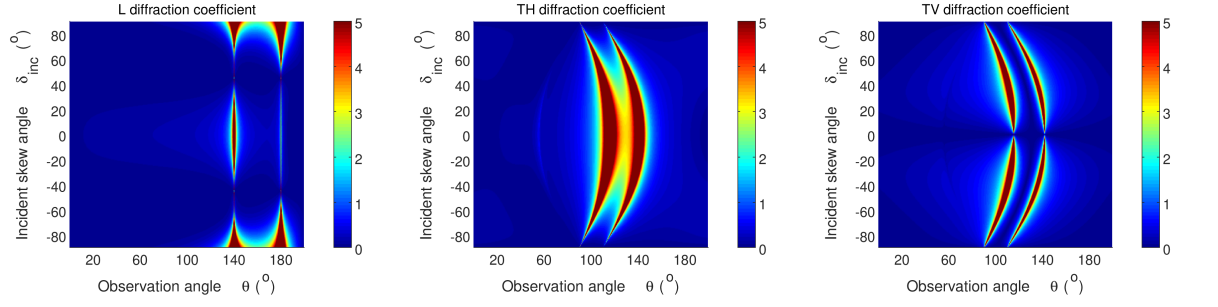

(a) Diffracted L wave (b) Diffracted TH wave (c) Diffracted TV wave

Fig. 15: Absolute value of the diffraction coefficient computed for an incident L wave on a wedge of angle $\varphi = 200^o$ with $\theta_{inc} = 40^o$

Conclusion

Using the spectral functions method, the elastic wave diffracted by a skew incident plane wave on an infinite stress-free wedge has been studied. In cases where Snell's law of diffraction yields a propagative wave for both longitudinal and transversal diffracted waves, a semi-analytical 3D computation method is developed theoretically and numerically, for all wedge angles. The corresponding 3D code has been tested in three different manners (by comparison to the 2D elastic code for 2D configurations, by testing the acoustic limit of the code and by computing the regular part in the case of reflection on an infinite plane), yielding promising results, but has yet to be validated (numerically or experimentally) for all 3D elastic cases. Further works should focus on the 3D diffraction of a transverse wave with skew angle above the critical one. The current work could also be extended for dealing with wedges of finite edge length [49].

Appendix A. Computation of the $\mathbb{D}_{l,k}$ matrix coefficients

The integral computations that are necessary to compute the coefficients of the matrices $\mathbb{D}$ and $\mathbb{T}$ which appear in the regular part of the spectral functions (see equations (4.36) and (4.39)) are given here. In all the following, $* = L, T$.

We begin by computing the coefficients of matrix $\mathbb{D}(a, b)$ defined by (4.36). The first step is to determine the value of a useful integral.

Appendix A.1. Integral $\int_{-1}^{1} \frac{\lambda t+\rho}{Q(t)}\, dt$

The following integral has already been computed in [42] and in [44]. The details of the computation will therefore not be repeated here, as they are a bit lengthy. We therefore only state the result, which is:

$$\int_{-1}^{1} \frac{\lambda t+\rho}{Q(t)}\, dt = \int_{-1}^{1} \frac{\lambda t+\rho}{iat^2+2\tilde{\nu}_* t-ia}\, dt = \frac{\lambda}{\tilde{\nu}_*}\mathrm{sog}(\frac{a}{\tilde{\nu}_*}) + i\frac{\rho}{\tilde{\nu}_*}\mathrm{rog}(\frac{a}{\tilde{\nu}_*}), \tag{A.1}$$

where rog and sog are two special functions defined for $a > 1$ by :

$$\mathrm{rog}(a) = \int_{-1}^{1} \frac{dx}{a(1-x^2)+2ix} = \frac{1}{\sqrt{a^2-1}} \log(a + \sqrt{a^2-1}) \tag{A.2}$$

and

$$\mathrm{sog}(a) = \frac{1}{a}\Big(\frac{\pi}{2} - \mathrm{rog}(a)\Big) \tag{A.3}$$

These functions may be extended to holomorphic functions on $\mathbb{C}\backslash\{-1\}$. Their properties are detailed in [42]. This result is used to determine the values of integrals I_1^* to I_6^* which appear in the coefficients of matrix $\mathbb{D}(a, b)$.

Appendix A.2. Integral I_1^*

Integral I_1^* is defined by :

$$\begin{aligned} I_1^* &= \int_{-\infty}^{+\infty} \frac{y}{(y+ib)(y-ia)\sqrt{\tilde{\nu}_*^2+y^2}}\, dy \\ &= \frac{1}{a+b}\left(\int_{-\infty}^{+\infty} \frac{b}{(y+ib)\sqrt{\tilde{\nu}_*^2+y^2}}\, dy + \int_{-\infty}^{+\infty} \frac{a}{(y-ia)\sqrt{\tilde{\nu}_*^2+y^2}}\, dy\right) \end{aligned} \tag{A.4}$$

This can be computed by applying the following variable change

$$y = 2\tilde{\nu}_* \tfrac{t}{1-t^2} \qquad \sqrt{\tilde{\nu}_*^2+y^2} = \tilde{\nu}_*\left(\tfrac{1+t^2}{1-t^2}\right) \qquad dy = 2\tilde{\nu}_* \tfrac{1+t^2}{(1-t^2)^2} dt \tag{A.5}$$

and using formula (A.1):

$$I_1^* = \frac{2ia}{(a+b)\tilde{\nu}_*}\mathrm{rog}(a/\tilde{\nu}_*) - \frac{2ib}{(a+b)\tilde{\nu}_*}\mathrm{rog}(b/\tilde{\nu}_*) \tag{A.6}$$

Appendix A.3. Integral I_2^*

Integral I_2^* is defined by :

$$I_2^* = \int_{-\infty}^{+\infty} \frac{y\sqrt{\tilde{\nu}_*^2 + y^2}}{(y+ib)(y-ia)}\, dy = \tilde{\nu}_*^2 I_1^* + I_3^* \tag{A.7}$$

where integrals I_1^* and I_3^* are defined by equations (A.4) and (A.8) and their expressions are given by (A.6) and (A.12) respectively.

Appendix A.4. Integral I_3^*

Integral I_3^* is defined by :

$$\begin{aligned} I_3^* &= \int_{-\infty}^{+\infty} \frac{y^3}{(y+ib)(y-ia)\sqrt{\tilde{\nu}_*^2 + y^2}}\, dy \\ &= \frac{b}{a+b}\int_{-\infty}^{+\infty} \frac{y^2}{(y+ib)\sqrt{\tilde{\nu}_*^2 + y^2}}\, dy + \frac{a}{a+b}\int_{-\infty}^{+\infty} \frac{y^2}{(y-ia)\sqrt{\tilde{\nu}_*^2 + y^2}}\, dy \end{aligned} \tag{A.8}$$

Each of these terms can be computed using variable change (A.5) :

$$\int_{-\infty}^{+\infty} \frac{y^2}{(y-ia)\sqrt{\tilde{\nu}_*^2 + y^2}}\, dy = \int_{-1}^{1} \frac{8\tilde{\nu}_*^2 t^2}{(1-t^2)^2(2\tilde{\nu}_* t - ia(1-t^2))}\, dt \tag{A.9}$$

The simple elements decomposition of the integrand is :

$$\frac{8\tilde{\nu}_*^2 t^2}{(1-t^2)^2(2\tilde{\nu}_* t - ia(1-t^2))} = \frac{ia}{1-t} + \frac{ia}{1+t} + \frac{\tilde{\nu}_*}{(1-t)^2} - \frac{\tilde{\nu}_*}{(1+t)^2} - \frac{2a^2}{2\tilde{\nu}_* t - ia(1-t^2)} \tag{A.10}$$

Using (A.1), we obtain

$$\frac{a}{a+b}\int_{-\infty}^{+\infty} \frac{y^2}{(y-ia)\sqrt{\tilde{\nu}_*^2 + y^2}}\, dy = \frac{2ia^2}{a+b}\log\left(\frac{1+t_{\tilde{\nu}_*}}{1-t_{\tilde{\nu}_*}}\right) - \frac{2ia^3}{\tilde{\nu}_*(a+b)}, \tag{A.11}$$

where $t_{\tilde{\nu}_*} \to 1$ is the upper bound of integral (A.9) after variable change (A.5) and will be discussed in the following. The value of $\int_{-\infty}^{+\infty} \frac{y^2}{(y+ib)\sqrt{\tilde{\nu}_*^2+y^2}}\, dy$ can be obtained in a similar manner. Finally:

$$I_3^* = 2i(a-b)\log\left(\frac{1+t_{\tilde{\nu}_*}}{1-t_{\tilde{\nu}_*}}\right) - \frac{2ia^3}{\tilde{\nu}_*(a+b)}\mathrm{rog}(a/\tilde{\nu}_*) + \frac{2ib^3}{\tilde{\nu}_*(a+b)}\mathrm{rog}(b/\tilde{\nu}_*) \tag{A.12}$$

Note the appearance of the term $\log\left(\frac{1+t_{\tilde{\nu}_*}}{1-t_{\tilde{\nu}_*}}\right)$ which diverges when $t_{\tilde{\nu}_*} \to 1$. This term will be compensated by another in the final expressions (Eqs. (A.25)-(A.28)) of the coefficients of matrix $\mathbb{D}$. In fact, (A.5) leads to :

$$\frac{2t_{\tilde{\nu}_*}}{1-t_{\tilde{\nu}_*}^2} = \frac{A}{\tilde{\nu}_*} \text{ and } A \to +\infty \text{ when } t_{\tilde{\nu}_*} \to 1 \tag{A.13}$$

Furthermore,

$$1 - t_{\tilde{\nu}_*} = \frac{(1-t_{\tilde{\nu}_*})(1+t_{\tilde{\nu}_*})}{1+t_{\tilde{\nu}_*}} \sim \frac{\tilde{\nu}_*}{A} \tag{A.14}$$

so that, when computing $I_3^L - I_3^T$ (for instance), the following term appears

$$\log\left(\frac{1+t_{\tilde{\nu}_L}}{1-t_{\tilde{\nu}_L}}\right) - \log\left(\frac{1+t_{\tilde{\nu}_T}}{1-t_{\tilde{\nu}_T}}\right) \sim \log(\tilde{\nu}_T/\tilde{\nu}_L) \tag{A.15}$$

Appendix A.5. Integral I_4^*

Integral I_4^* is defined by :

$$I_4^* = \int_{-\infty}^{+\infty} \frac{dy}{(y+ib)(y-ia)\sqrt{\tilde{\nu}_*^2+y^2}} \tag{A.16}$$

For $a+b \neq 0$,

$$\frac{1}{(y+ib)(y-ia)} = \frac{-i}{a+b}\left(\frac{1}{y-ia} - \frac{1}{y+ib}\right) \tag{A.17}$$

Substituting the above decomposition in (A.16) yields

$$I_4^* = \frac{i}{a+b}\int_{-\infty}^{+\infty}\left(\frac{1}{(y+ib)\sqrt{\tilde{\nu}_*^2+y^2}} - \frac{1}{(y-ia)\sqrt{\tilde{\nu}_*^2+y^2}}\right)dy \tag{A.18}$$

These integrals are computed using (A.1):

$$I_4^* = \frac{2}{\tilde{\nu}_*(a+b)}\left(\mathrm{rog}\,(a/\tilde{\nu}_*) + \mathrm{rog}\,(b/\tilde{\nu}_*)\right) \tag{A.19}$$

Appendix A.6. Integral I_5^*

Integral I_5^* is defined by :

$$I_5^* = \int_{-\infty}^{+\infty} \frac{y^2}{(y+ib)(y-ia)\sqrt{\tilde{\nu}_*^2+y^2}}\,dy \tag{A.20}$$

Using decomposition (A.17) yields

$$I_5^* = \frac{i}{a+b}\int_{-\infty}^{+\infty}\left(\frac{y^2}{(y+ib)\sqrt{\tilde{\nu}_*^2+y^2}} - \frac{y^2}{(y-ia)\sqrt{\tilde{\nu}_*^2+y^2}}\right)dy \tag{A.21}$$

These integrals have been computed at section Appendix A.4. Applying formula (A.11) yields:

$$I_5^* = 2\log\left(\frac{1+t_{\tilde{\nu}_*}}{1-t_{\tilde{\nu}_*}}\right) - \frac{2}{\tilde{\nu}_*(a+b)}[b^2\mathrm{rog}\,(b/\tilde{\nu}_*) + a^2\mathrm{rog}\,(a/\tilde{\nu}_*)] \tag{A.22}$$

Appendix A.7. Integral I_6^*

Integral I_6^* is defined by :

$$I_6^* = \int_{-\infty}^{+\infty} \frac{\sqrt{\tilde{\nu}_*^2+y^2}}{(y-ia)(y+ib)}\,dy = \tilde{\nu}_*^2 I_4^* + I_5^* \tag{A.23}$$

where integrals I_4^* and I_5^* are defined by equations (A.16) and (A.20) and their expressions are given by (A.19) and (A.22).

Appendix A.8. $\mathbb{D}_{lk}$ matrix coefficients

The first coefficient can be computed using Gauss' integral formula :

$$\mathcal{D}_1(a,b) = \int_{-\infty}^{+\infty} \frac{dy}{(y+ib)(y-ia)} = \frac{2\pi}{a+b} \tag{A.24}$$

The two other coeffcients are linear combinations of integrals I_1^* to I_6^* :

$$\begin{aligned}\mathcal{D}_2^L(a,b) &= \int_{-\infty}^{+\infty} \frac{iy[1-2\mu(\zeta_L(iy)\zeta_T(iy) - y^2+\tau^2)]}{(y+ib)(y-ia)\zeta_L(iy)}\,dy \\ &= -i(1-2\mu\tau^2)I_1^L + 2i\mu(I_2^T - I_3^L)\end{aligned} \tag{A.25}$$

$$\mathcal{D}_2^T(a,b) = \int_{-\infty}^{+\infty} \frac{iy[1-2\mu(\zeta_L(iy)\zeta_T(iy)-y^2+\tau^2)]}{(y+ib)(y-ia)\zeta_T(iy)}\,dy = -i(1-2\mu\tau^2)I_1^T + 2i\mu(I_2^L - I_3^T) \tag{A.26}$$

$$\mathcal{D}_3^L(a,b) = \tau\int_{-\infty}^{+\infty} \frac{1-2\mu(\zeta_L(iy)\zeta_T(iy)-y^2+\tau^2)}{(y+ib)(y-ia)\zeta_L(iy)}\,dy = -\tau(1-2\mu\tau^2)I_4^L - 2\mu\tau I_5^L + 2\mu\tau I_6^T \tag{A.27}$$

$$\mathcal{D}_3^T(a,b) = \tau\int_{-\infty}^{+\infty} \frac{1-2\mu(\zeta_L(iy)\zeta_T(iy)-y^2+\tau^2)}{(y+ib)(y-ia)\zeta_T(iy)}\,dy = -\tau(1-2\mu\tau^2)I_4^T - 2\mu\tau I_5^T + 2\mu\tau I_6^L \tag{A.28}$$

This concludes computation of matrix coefficients $\mathbb{D}_{lk}$.

Appendix B. Computation of the $\mathbb{T}_{l,k}$ matrix coefficients

Let us now compute the coefficients of matrix $\mathbb{T}(a,b)$, defined by (4.39). A number of the integrals which appear in these coefficients (specifically integrals J_1^* to J_5^*) have already been defined and computed in the article concerning the 2D elastic case [44]. As the computations are quite lengthy, only the results will be stated here and we only detail the computations for the integrals which have not appeared before.

As a first step, an additional integral is defined and its value will be used in the subsequent computations.

Appendix B.1. Integral $\int_{-1}^{1} \frac{\eta t+\psi}{P(t)}\,dt$

Let us define the following integral, which has been computed in [42] and [44]:

$$\int_{-1}^{1} \frac{\eta t+\psi}{P(t)}\,dt = \int_{-1}^{1} \frac{\eta t+\psi}{(\tilde{\nu}_*\sin\tilde{\varphi}-b)t^2 - 2i\tilde{\nu}_* t\cos\tilde{\varphi}} = \frac{i\eta}{\tilde{\nu}_*\sin\tilde{\varphi}-b}[\tilde{\varphi}-\frac{\pi}{2}+\cos\tilde{\varphi}\,\mathrm{rog}(\frac{b}{\tilde{\nu}_*})] + \frac{\psi}{\tilde{\nu}_*}\mathrm{rog}(\frac{b}{\tilde{\nu}_*}) \tag{B.1}$$

Let us now use these results to compute some more complex integrals.

Appendix B.2. Integral J_1^*

Integral J_1^* is defined by :

$$J_1^* = \int_{-\infty}^{+\infty} \frac{y(\tilde{\nu}_*^2+y^2)}{(y-ia)[b-iy\cos\varphi+\sqrt{\tilde{\nu}_*^2+y^2}\sin\tilde{\varphi})]\sqrt{\tilde{\nu}_*^2+y^2}}\,dy = \tilde{\nu}_*^2 J_5^* + J_4^* \tag{B.2}$$

where integral J_4^* and J_5^* are defined by equations (B.15) and (B.19) and their expressions are given (B.18) and (B.22) respectively.

Appendix B.3. Integral J_2^*

Integral J_2^* is defined by :

$$J_2^* = \int_{-\infty}^{+\infty} \frac{y^2}{(y-ia)[b-iy\cos\tilde{\varphi}+\sqrt{\tilde{\nu}_*^2+y^2}\sin\tilde{\varphi})]}\,dy \tag{B.3}$$

Once more, the variable change (A.5) is applied :

$$J_2^* = 8\tilde{\nu}_*^3\int_{-1}^{1} \frac{t^2(t^2+1)}{(1-t^2)^2[b(1-t^2)-2\tilde{\nu}_* it\cos\tilde{\varphi}+\sin\tilde{\varphi}\tilde{\nu}_*(1+t^2)](2\tilde{\nu}_* t - ia(1-t^2))}\,dt \tag{B.4}$$

The simple elements decomposition of the integrand is :

$$\frac{8\tilde{\nu}_*^3 t^2(1+t^2)}{(1-t)^2(1+t)^2P(t)Q(t)} = \frac{be^{-2i\tilde{\varphi}}-ae^{-i\tilde{\varphi}}}{1-t} + \frac{ae^{i\tilde{\varphi}}-be^{2i\tilde{\varphi}}}{1+t} + \frac{\tilde{\nu}_* e^{i(\pi/2-\tilde{\varphi})}}{(1-t)^2} + \frac{\tilde{\nu}_* e^{i(\pi/2+\tilde{\varphi})}}{(1+t)^2} + \frac{\eta_2 t+\psi_2}{P(t)} + \frac{\lambda_2 t+\rho_2}{Q(t)} \tag{B.5}$$

where Q and P are defined by (A.1) and (B.1).

Let $N(t)$ be a third degree polynomial such that :

$$\frac{\eta t+\psi}{P(t)}+\frac{\lambda t+\rho}{Q(t)}=\frac{N(t)}{P(t)Q(t)} \tag{B.6}$$

Then the coefficients of the simple elements decomposition are given by :

$$\begin{cases}\eta=\frac{1}{p_+-p_-}\left[\frac{N(p_+)}{Q(p_+)}-\frac{N(p_-)}{Q(p_-)}\right]\\ \psi=\frac{N(p_+)}{Q(p_+)}-\eta p_+\end{cases}\text{ and }\begin{cases}\lambda=\frac{1}{q_+-q_-}\left[\frac{N(q_+)}{P(q_+)}-\frac{N(q_-)}{P(q_-)}\right]\\ \rho=\frac{N(q_+)}{P(q_+)}-\lambda q_+\end{cases}, \tag{B.7}$$

where $p_\pm$ and $q_\pm$ are respectively the roots of polynomials P and Q and are defined by:

$$q_\pm=\frac{1}{a}(i\tilde{\nu}_*\pm\sqrt{a^2-\tilde{\nu}_*^2}) \tag{B.8}$$

and

$$p_\pm=\frac{\tilde{\nu}_* i\cos\tilde{\varphi}\pm\sqrt{b^2-\tilde{\nu}_*^2}}{\tilde{\nu}_*\sin\varphi-b} \tag{B.9}$$

η_2,ψ_2,λ_2 and ρ_2 are obtained using (B.5) and (B.7). The final result is obtained using (A.1) and (B.1) :

$$\begin{aligned}J_2^*\sim{}&2i\cos\tilde{\varphi}A+2i(a\sin\tilde{\varphi}-b\sin(2\tilde{\varphi}))\ln\left(\frac{1+t_{\tilde{\nu}_*}}{1-t_{\tilde{\nu}_*}}\right)\\&+\frac{8i\eta_2\tilde{\nu}_*^2}{b/\tilde{\nu}_*-\sin\tilde{\varphi}}\left(\frac{\pi}{2}-\tilde{\varphi}-\cos\tilde{\varphi}\,\mathrm{rog}(\frac{b}{\tilde{\nu}_*})\right)+8\tilde{\nu}_*^2\psi_2\mathrm{rog}(\frac{b}{\tilde{\nu}_*})+8\tilde{\nu}_*^2\left(\lambda_2\mathrm{sog}(a/\tilde{\nu}_*)+i\rho_2\mathrm{rog}(a/\tilde{\nu}_*)\right),\end{aligned} \tag{B.10}$$

where $A\to+\infty$ and $t_{\tilde{\nu}_*}\to 1$. These diverging terms will be compensated by others when the contributions of $\mathcal{T}^T$ and $\mathcal{T}^L$ will be summed, according to (A.15).

Appendix B.4. Integral J_3^*

J_3^* is defined by :

$$J_3^*=\int_{-\infty}^{+\infty}\frac{1}{(y-ia)[b-iy\cos\tilde{\varphi}+\sqrt{\tilde{\nu}_*^2+y^2}\sin\tilde{\varphi}]}\,dy \tag{B.11}$$

Variable change (A.5) is applied:

$$J_3^*=2\tilde{\nu}_*\int_{-1}^{1}\frac{1+t^2}{(2\tilde{\nu}_* t-ia(1-t^2))(b(1-t^2)-2i\tilde{\nu}_* t\cos\tilde{\varphi}+\tilde{\nu}_*\sin\tilde{\varphi}(1+t^2))}\,dt \tag{B.12}$$

The simple elements decomposition is of the form

$$\frac{1+t^2}{P(t)Q(t)}=\frac{\eta_3 t+\psi_3}{P(t)}+\frac{\lambda_3 t+\rho_3}{Q(t)} \tag{B.13}$$

The coefficients are computed using (B.7), yielding :

$$J_3^*=\frac{2i\eta_3}{b/\tilde{\nu}_*-\sin\tilde{\varphi}}\left(\frac{\pi}{2}-\tilde{\varphi}-\cos\tilde{\varphi}\,\mathrm{rog}(\frac{b}{\tilde{\nu}_*})\right)+2\psi_3\mathrm{rog}(\frac{b}{\tilde{\nu}_*})+2\left(\lambda_3\mathrm{sog}(a/\tilde{\nu}_*)+i\rho_3\mathrm{rog}(a/\tilde{\nu}_*)\right) \tag{B.14}$$

Appendix B.5. Integral J_4^*

J_4^* is defined by :

$$J_4^*=\int_{-\infty}^{+\infty}\frac{y^3}{(y-ia)\sqrt{y^2+\tilde{\nu}_*^2}(b-iy\cos\tilde{\varphi}+\sqrt{\tilde{\nu}_*^2+y^2}\sin\tilde{\varphi})}\,dy \tag{B.15}$$

Variable change (A.5) is applied :

$$J_4^* = 16\tilde{\nu}_*^3 \int_{-1}^{1} \frac{t^3}{(2\tilde{\nu}_* t - ia(1-t^2))(1-t^2)^2(b(1-t^2) - 2i\tilde{\nu}_* t\cos\tilde{\varphi} + \tilde{\nu}_*(1+t^2)\sin\tilde{\varphi})}\, dt \tag{B.16}$$

The simple elements decomposition is

$$\frac{16\tilde{\nu}_*^3 t^3}{(1-t^2)^2 P(t)Q(t)} = \frac{be^{-2i\tilde{\varphi}} - ae^{-i\tilde{\varphi}}}{1-t} + \frac{be^{2i\tilde{\varphi}} - ae^{i\tilde{\varphi}}}{1+t} + \frac{\tilde{\nu}_* e^{i(\pi/2-\tilde{\varphi})}}{(1-t)^2} + \frac{\tilde{\nu}_* e^{i(\tilde{\varphi}-\pi/2)}}{(1+t)^2} + \frac{\eta_4 t + \psi_4}{P(t)} + \frac{\lambda_4 t + \rho_4}{Q(t)}, \tag{B.17}$$

Coefficients $\eta_4, \psi_4, \lambda_4, \rho_4$ are determined using (B.7), and finally :

$$\begin{aligned} J_4^* \sim\ & 2A\sin\tilde{\varphi} + 2(b\cos(2\tilde{\varphi}) - a\cos\tilde{\varphi})\ln\left(\frac{1+t_{\tilde{\nu}_*}}{1-t_{\tilde{\nu}_*}}\right) \\ & + \frac{16i\eta_4\tilde{\nu}_*^2}{b/\tilde{\nu}_* - \sin\tilde{\varphi}}\left(\frac{\pi}{2} - \tilde{\varphi} - \cos\tilde{\varphi}\,\mathrm{rog}(\frac{b}{\tilde{\nu}_*})\right) + 16\tilde{\nu}_*^2\psi_4\mathrm{rog}(\frac{b}{\tilde{\nu}_*}) + 16\tilde{\nu}_*^2\left(\lambda_4\mathrm{sog}(a/\tilde{\nu}_*) + i\rho_4\mathrm{rog}(a/\tilde{\nu}_*)\right) \end{aligned} \tag{B.18}$$

Appendix B.6. Integral J_5^*

J_5^* is defined by

$$J_5^* = \int_{-\infty}^{+\infty} \frac{y}{(y-ia)\sqrt{\tilde{\nu}_*^2 + y^2}[b - (iy\cos\tilde{\varphi} + \zeta_*(iy)\sin\tilde{\varphi})]}\, dy \tag{B.19}$$

Variable change (A.5) is applied :

$$J_5^* = 4\tilde{\nu}_* \int_{-1}^{1} \frac{t}{P(t)Q(t)}\, dt \tag{B.20}$$

The simple elements decomposition is of the form

$$\frac{t}{P(t)Q(t)} = \frac{\eta_5 t + \psi_5}{P(t)} + \frac{\lambda_5 t + \rho_5}{Q(t)} \tag{B.21}$$

The coefficients $\eta_5, \psi_5, \lambda_5, \rho_5$ are computed using (B.7), yielding:

$$J_5^* = \frac{4i\eta_5}{b/\tilde{\nu}_* - \sin\tilde{\varphi}}\left(\frac{\pi}{2} - \tilde{\varphi} - \cos\tilde{\varphi}\,\mathrm{rog}(\frac{b}{\tilde{\nu}_*})\right) + 4\psi_5\mathrm{rog}(\frac{b}{\tilde{\nu}_*}) + 4\left(\lambda_5\mathrm{sog}(a/\tilde{\nu}_*) + i\rho_5\mathrm{rog}(a/\tilde{\nu}_*)\right) \tag{B.22}$$

Appendix B.7. Integral J_6^*

Integral J_6^* is defined by

$$J_6^* = \int_{-\infty}^{+\infty} \frac{y}{(y-ia)[b - (iy\cos\tilde{\varphi} + \zeta_*(iy)\sin\tilde{\varphi})]}\, dy \tag{B.23}$$

Variable change (A.5) is applied

$$J_6^* = 4\tilde{\nu}_*^2 \int_{-1}^{1} \frac{t(1+t^2)}{(1-t^2)P(t)Q(t)}\, dt \tag{B.24}$$

The simple elements decomposition is of the form

$$\frac{t(1+t^2)}{(1-t^2)P(t)Q(t)} = \frac{e^{i(\pi/2-\tilde{\varphi})}}{4\tilde{\nu}_*^2(1-t)} + \frac{e^{-i(\pi/2-\tilde{\varphi})}}{4\tilde{\nu}_*^2(1+t)} + \frac{\eta_6 t + \psi_6}{P(t)} + \frac{\lambda_6 t + \rho_6}{Q(t)} \tag{B.25}$$

Subtracting the first two terms of the simple elements decomposition from both sides of this equation yields

$$\begin{aligned} \frac{\eta_6 t + \psi_6}{P(t)} + \frac{\lambda_6 t + \rho_6}{Q(t)} =\ & -\frac{(\sin\tilde{\varphi} + i\cos\tilde{\varphi}t)}{2\tilde{\nu}_*^2 P(t)Q(t)}\Big(b(2\tilde{\nu}_* t - ia(1-t^2)) - a\tilde{\nu}_*(2\cos\tilde{\varphi}t + i\sin\tilde{\varphi}(1+t^2))\Big) \\ & + \frac{\cos^2\tilde{\varphi}.t + i\sin\tilde{\varphi}\cos\tilde{\varphi}.t^2}{P(t)Q(t)} \end{aligned} \tag{B.26}$$

The final coefficients are determined using (B.7). Finally:

$$J_6^* = 2\sin\tilde{\varphi}\ln\left(\frac{1+t_{\tilde{\nu}_*}}{1-t_{\tilde{\nu}_*}}\right) + \frac{4i\eta_6\tilde{\nu}_*}{b/\tilde{\nu}_* - \sin\tilde{\varphi}}\left(\frac{\pi}{2} - \tilde{\varphi} - \cos\tilde{\varphi}\,\mathrm{rog}(\frac{b}{\tilde{\nu}_*})\right) + 4\tilde{\nu}_*\psi_6\mathrm{rog}(\frac{b}{\tilde{\nu}_*}) + 4\tilde{\nu}_*\left(\lambda_6\mathrm{sog}(a/\tilde{\nu}_*) + i\rho_6\mathrm{rog}(a/\tilde{\nu}_*)\right) \tag{B.27}$$

Appendix B.8. Integral J_7^*

Integral J_7^* is defined by

$$J_7^* = \int_{-\infty}^{+\infty} \frac{y^2}{(y - ia)\sqrt{\tilde{\nu}_*^2 + y^2}[b - (iy\cos\tilde{\varphi} + \zeta_*(iy)\sin\tilde{\varphi})]}\, dy \tag{B.28}$$

Variable change (A.5) is applied

$$J_7^* = 8\tilde{\nu}_*^2 \int_{-1}^{1} \frac{t^2}{(1-t^2)P(t)Q(t)}\, dt \tag{B.29}$$

The simple elements decomposition is of the form

$$\frac{t^2}{(1-t^2)P(t)Q(t)} = \frac{e^{i(\frac{\pi}{2}-\tilde{\varphi})}}{8\tilde{\nu}_*^2(1-t)} + \frac{e^{i(\frac{\pi}{2}+\tilde{\varphi})}}{8\tilde{\nu}_*^2(1+t)} + \frac{\eta_7 t + \psi_7}{P(t)} + \frac{\lambda_7 t + \rho_7}{Q(t)} \tag{B.30}$$

The remaining terms are

$$\begin{aligned}\frac{\eta_7 t + \psi_7}{P(t)} + \frac{\lambda_7 t + \rho_7}{Q(t)} = &-\frac{(i\cos\tilde{\varphi} + \sin\tilde{\varphi}t)}{4\tilde{\nu}_*^2 P(t)Q(t)}[b(2\tilde{\nu}_* t - ia(1-t^2)) - a\tilde{\nu}_*(2\cos\tilde{\varphi}t + i\sin\tilde{\varphi}(1+t^2))] \\ &+ \frac{\sin^2\tilde{\varphi}t^2 - i\cos\tilde{\varphi}\sin\tilde{\varphi}t}{2P(t)Q(t)}\end{aligned} \tag{B.31}$$

The final coefficients are determined using (B.7). Finally:

$$J_7^* \sim 2i\cos\tilde{\varphi}\log\left(\frac{1+t_{\tilde{\nu}_*}}{1-t_{\tilde{\nu}_*}}\right) + \frac{8i\eta_7\tilde{\nu}_*}{b/\tilde{\nu}_* - \sin\tilde{\varphi}}\left(\frac{\pi}{2} - \tilde{\varphi} - \cos\tilde{\varphi}\,\mathrm{rog}(\frac{b}{\tilde{\nu}_*})\right) + 8\tilde{\nu}_*\psi_7\mathrm{rog}(\frac{b}{\tilde{\nu}_*}) + 8\tilde{\nu}_*\left(\lambda_7\mathrm{sog}(a/\tilde{\nu}_*) + i\rho_7\mathrm{rog}(a/\tilde{\nu}_*)\right) \tag{B.32}$$

Appendix B.9. Integral J_8^*

Integral J_8^* is defined by

$$J_8^* = \int_{-\infty}^{+\infty} \frac{dy}{(y - ia)\sqrt{\tilde{\nu}_*^2 + y^2}[b - (iy\cos\tilde{\varphi} + \zeta_*(iy)\sin\tilde{\varphi})]} \tag{B.33}$$

Variable change (A.5) is applied

$$J_8^* = 2\int_{-1}^{1} \frac{1-t^2}{P(t)Q(t)}\, dt \tag{B.34}$$

The simple elements decomposition is of the form

$$\frac{1-t^2}{P(t)Q(t)} = \frac{\eta_8 t + \psi_8}{P(t)} + \frac{\lambda_8 t + \rho_8}{Q(t)} \tag{B.35}$$

The final coefficients are determined using (B.7). Finally:

$$J_8^* = \frac{2i\eta_8}{b - \tilde{\nu}_*\sin\tilde{\varphi}}\left(\frac{\pi}{2} - \tilde{\varphi} - \cos\tilde{\varphi}\,\mathrm{rog}(\frac{b}{\tilde{\nu}_*})\right) + 2\frac{\psi_8}{\tilde{\nu}_*}\mathrm{rog}(\frac{b}{\tilde{\nu}_*}) + \frac{2}{\tilde{\nu}_*}\left(\lambda_8\mathrm{sog}(a/\tilde{\nu}_*) + i\rho_8\mathrm{rog}(a/\tilde{\nu}_*)\right) \tag{B.36}$$

Appendix B.10. $\mathbb{T}_{kl}$ matrix coefficients

The coefficients of matrices $\mathbb{T}_{lk}$ are linear combinations of integrals J_1^* to J_8^*. These linear combinations are given in the sequel.

Appendix B.10.1. L terms

We begin by computing the terms derived from $\mathbf{tm}_L$, defined by (4.12).

$$\begin{aligned}\mathcal{T}_1^L(a,b) &= \mu\int_{-\infty}^{+\infty}\frac{iy[2i\epsilon\cos(2\varphi).y\zeta_L(iy)+\sin(2\varphi)(y^2+\zeta_L^2(iy))]}{(y-ia)\zeta_L(iy)[b-(iy\cos\varphi+\zeta_L(iy)\sin\tilde{\varphi})]}\,dy\\ &= -2\epsilon\mu\cos(2\varphi)J_2^L - i\mu\sin(2\varphi)(J_1^L+J_4^L)\end{aligned} \tag{B.37}$$

$$\begin{aligned}\mathcal{T}_2^L(a,b) &= \mu\int_{-\infty}^{+\infty}\frac{2i\cos(2\varphi).y\zeta_L(iy)+\epsilon\sin(2\varphi)(y^2+\zeta_L^2(iy))}{(y-ia)[b-(iy\cos\varphi+\zeta_L(iy)\sin\tilde{\varphi})]}\,dy\\ &= -2i\mu\cos(2\varphi)J_1^L + \epsilon\mu\sin(2\varphi)(2J_2^L+\tilde{\nu}_L^2J_3^L)\end{aligned} \tag{B.38}$$

$$\begin{aligned}\mathcal{T}_3^L(a,b) &= \mu\tau\int_{-\infty}^{+\infty}\frac{2i\epsilon\cos(2\varphi).y\zeta_L(iy)+\sin(2\varphi)(y^2+\zeta_L^2(iy))}{(y-ia)\zeta_L(iy)[b-(iy\cos\varphi+\zeta_L(iy)\sin\tilde{\varphi})]}\,dy\\ &= \mu\tau[2i\epsilon\cos(2\varphi)J_6^L - \sin(2\varphi)(2J_7^L+\tilde{\nu}_L^2J_8^L)]\end{aligned} \tag{B.39}$$

$$\begin{aligned}\mathcal{T}_4^L(a,b) &= (2\mu-1)\int_{-\infty}^{+\infty}\frac{iy}{(y-ia)\zeta_L(iy)[b-(iy\cos\varphi+\zeta_L(iy)\sin\tilde{\varphi})]}\,dy\\ &\quad+2\mu\int_{-\infty}^{+\infty}\frac{iy[i\epsilon\sin(2\varphi).y\zeta_L(iy)-\zeta_L^2(iy)\cos^2\varphi+y^2\sin^2\varphi]}{(y-ia)\zeta_L(iy)[b-(iy\cos\varphi+\zeta_L(iy)\sin\tilde{\varphi})]}\,dy\\ &= i(1-2\mu)J_5^L + 2i\mu\cos^2\varphi J_1^L - 2\epsilon\mu\sin(2\varphi)J_2^L - 2i\mu\sin^2\varphi J_4^L\end{aligned} \tag{B.40}$$

$$\begin{aligned}\mathcal{T}_5^L(a,b) &= (2\mu-1)\int_{-\infty}^{+\infty}\frac{\epsilon}{(y-ia)[b-(iy\cos\varphi+\zeta_L(iy)\sin\tilde{\varphi})]}\,dy\\ &\quad+2\mu\int_{-\infty}^{+\infty}\frac{i\sin(2\varphi).y\zeta_L(iy)-\epsilon\cos^2\varphi\zeta_L^2(iy)+\epsilon\sin^2\varphi y^2}{(y-ia)[b-(iy\cos\varphi+\zeta_L(iy)\sin\tilde{\varphi})]}\,dy\\ &= \epsilon(2\mu-1-2\mu\tilde{\nu}_L^2\cos^2\varphi)J_3^L - 2i\mu\sin(2\varphi)J_1^L - 2\epsilon\mu\cos(2\varphi)J_2^L\end{aligned} \tag{B.41}$$

$$\begin{aligned}\mathcal{T}_6^L(a,b) &= \int_{-\infty}^{+\infty}\frac{\tau(2\mu-1)}{(y-ia)\zeta_L(iy)[b-(iy\cos\varphi+\zeta_L(iy)\sin\tilde{\varphi})]}\,dy\\ &\quad+2\mu\tau\int_{-\infty}^{+\infty}\frac{i\epsilon\sin(2\varphi).y\zeta_L(iy)-\cos^2\varphi\zeta_L^2(iy)+\sin^2\varphi y^2}{(y-ia)\zeta_L(iy)[b-(iy\cos\varphi+\zeta_L(iy)\sin\tilde{\varphi})]}\,dy\\ &= \tau(\lambda+2\mu\tilde{\nu}_L^2\cos^2\varphi)J_8^L + 2\mu\tau[i\epsilon\sin(2\varphi)J_6^L+\cos(2\varphi)J_7^L]\end{aligned} \tag{B.42}$$

$$\begin{aligned}\mathcal{T}_7^L(a,b) &= -2\mu\tau\int_{-\infty}^{+\infty}\frac{\epsilon iy\zeta_L(iy)\cos\varphi+y^2\sin\varphi}{(y-ia)\zeta_L(iy)[b-(iy\cos\varphi+\zeta_L(iy)\sin\tilde{\varphi})]}\,dy\\ &= -2\mu\tau(\sin\varphi J_7^L - i\epsilon\cos\varphi J_6^L)\end{aligned} \tag{B.43}$$

$$\begin{aligned}\mathcal{T}_8^L(a,b) &= -2\mu\tau\int_{-\infty}^{+\infty}\frac{i\epsilon y\sin\varphi-\zeta_L(iy)\cos\varphi}{(y-ia)[b-(iy\cos\varphi+\zeta_L(iy)\sin\tilde{\varphi})]}\,dy\\ &= -2\mu\tau[i\epsilon\sin\varphi J_6^L + \cos\varphi(J_7^L+\tilde{\nu}_L^2J_8^L)]\end{aligned} \tag{B.44}$$

$$\begin{aligned}\mathcal{T}_9^L(a,b) &= 2\mu\tau^2\int_{-\infty}^{+\infty}\frac{iy\sin\varphi-\epsilon\zeta_L(iy)\cos\varphi}{(y-ia)\zeta_L(iy)[b-(iy\cos\varphi+\zeta_L(iy)\sin\tilde{\varphi})]}\,dy\\ &= 2\mu\tau^2[i\sin\varphi J_5^L + \epsilon\cos\varphi J_3^L]\end{aligned} \tag{B.45}$$

Appendix B.10.2. TH terms

Let us now compute terms derived from $\mathbf{tm}_{TH}$, defined by (4.13).

$$\begin{aligned}\mathcal{T}_1^{TH}(a,b) &= \mu\left(1+\frac{\tau^2}{\tilde{\nu}_T^2}\right)\int_{-\infty}^{+\infty}\frac{-2i\sin(2\varphi).y\zeta_T(iy)+\epsilon\cos(2\varphi)(y^2+\zeta_T^2(iy))}{(y-ia)[b-(iy\cos\varphi+\zeta_T(iy)\sin\tilde{\varphi})]}\,dy\\ &= \mu\left(1+\frac{\tau^2}{\tilde{\nu}_T^2}\right)[2i\sin(2\varphi)J_1^T+\epsilon\cos(2\varphi)(2J_2^T+\tilde{\nu}_T^2J_3^T)]\end{aligned} \tag{B.46}$$

$$\begin{aligned}\mathcal{T}_2^{TH}(a,b) &= \mu\left(1+\frac{\tau^2}{\tilde{\nu}_T^2}\right)\int_{-\infty}^{+\infty}\frac{iy[2i\epsilon\sin(2\varphi).y\zeta_T(iy)-\cos(2\varphi)(y^2+\zeta_T^2(iy))]}{(y-ia)\zeta_T(iy)[b-(iy\cos\varphi+\zeta_T(iy)\sin\tilde{\varphi})]}\,dy\\ &= \mu\left(1+\frac{\tau^2}{\tilde{\nu}_T^2}\right)[-2\epsilon\sin(2\varphi)J_2^T+i\cos(2\varphi)(J_1^T+J_4^T)]\end{aligned} \tag{B.47}$$

$$\begin{aligned}\mathcal{T}_4^{TH}(a,b) &= \mu\left(1+\frac{\tau^2}{\tilde{\nu}_T^2}\right)\int_{-\infty}^{+\infty}\frac{2i\cos(2\varphi).y\zeta_T(iy)+\epsilon\sin(2\varphi)(y^2+\zeta_T^2(iy))}{(y-ia)[b-(iy\cos\varphi+\zeta_T(iy)\sin\tilde{\varphi})]}\,dy\\ &= \mu\left(1+\frac{\tau^2}{\tilde{\nu}_T^2}\right)[-2i\cos(2\varphi)J_1^T+\epsilon\sin(2\varphi)(2J_2^T+\tilde{\nu}_TJ_3^T)]\end{aligned} \tag{B.48}$$

$$\begin{aligned}\mathcal{T}_5^{TH}(a,b) &= \mu\left(1+\frac{\tau^2}{\tilde{\nu}_T^2}\right)\int_{-\infty}^{+\infty}\frac{-iy[2i\epsilon\cos(2\varphi).y\zeta_T(iy)+\sin(2\varphi)(y^2+\zeta_T^2(iy))]}{(y-ia)\zeta_T(iy)[b-(iy\cos\varphi+\zeta_T(iy)\sin\tilde{\varphi})]}\,dy\\ &= \mu\left(1+\frac{\tau^2}{\tilde{\nu}_T^2}\right)[2\epsilon\cos(2\varphi)J_2^T+i\sin(2\varphi)(J_1^T+J_4^T)]\end{aligned} \tag{B.49}$$

$$\begin{aligned}\mathcal{T}_7^{TH}(a,b) &= \mu\tau\left(1+\frac{\tau^2}{\tilde{\nu}_T^2}\right)\int_{-\infty}^{+\infty}\frac{\sin\varphi\zeta_T(iy)+i\epsilon\cos\varphi.y}{(y-ia)[b-(iy\cos\varphi+\zeta_T(iy)\sin\tilde{\varphi})]}\\ &= -\mu\tau\left(1+\frac{\tau^2}{\tilde{\nu}_T^2}\right)[i\epsilon\cos\varphi J_6^T-\sin\varphi(J_7^T+\tilde{\nu}_T^2J_8^T)]\end{aligned} \tag{B.50}$$

$$\begin{aligned}\mathcal{T}_8^{TH}(a,b) &= \mu\tau\left(1+\frac{\tau^2}{\tilde{\nu}_T^2}\right)\int_{-\infty}^{+\infty}\frac{\cos\varphi.y^2-i\epsilon\sin\varphi.y\zeta_T(iy)}{(y-ia)\zeta_T(iy)[b-(iy\cos\varphi+\zeta_T(iy)\sin\tilde{\varphi})]}\\ &= \mu\tau\left(1+\frac{\tau^2}{\tilde{\nu}_T^2}\right)[i\epsilon\sin\varphi J_6^T+\cos\varphi J_7^T]\end{aligned} \tag{B.51}$$

In addition, we have

$$\mathcal{T}_3^{TH}=\mathcal{T}_6^{TH}=\mathcal{T}_9^{TH}=0$$

Appendix B.10.3. TV terms

Finally, we compute terms derived from $\mathbf{tm}_{TV}$, defined by (4.14).

$$\begin{aligned}\mathcal{T}_1^{TV}(a,b) &= \mu\frac{\tau^2}{\tilde{\nu}_T^2}\int_{-\infty}^{+\infty}\frac{iy[2i\epsilon\cos(2\varphi).y\zeta_T(iy)+\sin(2\varphi)(y^2+\zeta_T^2(iy))]}{(y-ia)\zeta_T(iy)[b-(iy\cos\varphi+\zeta_T(iy)\sin\tilde{\varphi})]}\,dy\\ &= -\mu\frac{\tau^2}{\tilde{\nu}_T^2}[2\epsilon\cos(2\varphi)J_2^T+i\sin(2\varphi)(J_1^T+J_4^T)]\end{aligned} \tag{B.52}$$

$$\mathcal{T}_2^{TV}(a,b) = \mu\frac{\tau^2}{\tilde{\nu}_T^2}\int_{-\infty}^{+\infty}\frac{2i\cos(2\varphi).y\zeta_T(iy) + \epsilon\sin(2\varphi)(y^2+\zeta_T^2(iy))}{(y-ia)[b-(iy\cos\varphi+\zeta_T(iy)\sin\tilde{\varphi})]}\,dy$$
$$= \mu\frac{\tau^2}{\tilde{\nu}_T^2}[-2i\cos(2\varphi)J_1^T + \epsilon\sin(2\varphi)(2J_2^T + \tilde{\nu}_T^2 J_3^T)] \tag{B.53}$$

$$\mathcal{T}_3^{TV}(a,b) = -\mu\tau\int_{-\infty}^{+\infty}\frac{2i\epsilon\cos(2\varphi).y\zeta_T(iy) + \sin(2\varphi)(y^2+\zeta_T^2(iy))}{(y-ia)\zeta_L(iy)[b-(iy\cos\varphi+\zeta_T(iy)\sin\tilde{\varphi})]}\,dy$$
$$= \mu\tau[\sin(2\varphi)(2J_7^T + \tilde{\nu}_T^2 J_8^T) - 2i\epsilon\cos(2\varphi)J_6^T] \tag{B.54}$$

$$\mathcal{T}_4^{TV}(a,b) = 2\mu\frac{\tau^2}{\tilde{\nu}_T^2}\int_{-\infty}^{+\infty}\frac{iy[i\epsilon\sin(2\varphi).y\zeta_T(iy) - \zeta_T^2(iy)\cos^2\varphi + y^2\sin^2\varphi]}{(y-ia)\zeta_T(iy)[b-(iy\cos\varphi+\zeta_T(iy)\sin\tilde{\varphi})]}\,dy$$
$$= 2\mu\frac{\tau^2}{\tilde{\nu}_T^2}[i\cos^2\varphi J_1^T - \epsilon\sin(2\varphi)J_2^T - i\sin^2\varphi J_4^T] \tag{B.55}$$

$$\mathcal{T}_5^{TV}(a,b) = 2\mu\frac{\tau^2}{\tilde{\nu}_T^2}\int_{-\infty}^{+\infty}\frac{i\sin(2\varphi).y\zeta_T(iy) - \epsilon\cos^2\varphi\zeta_T^2(iy) + \epsilon\sin^2\varphi y^2}{(y-ia)[b-(iy\cos\varphi+\zeta_T(iy)\sin\tilde{\varphi})]}\,dy$$
$$= -2\mu\frac{\tau^2}{\tilde{\nu}_T^2}[i\sin(2\varphi)J_1^T + \epsilon\cos(2\varphi)J_2^T + \tilde{\nu}_T^2\cos^2\varphi J_3^T] \tag{B.56}$$

$$\mathcal{T}_6^{TV}(a,b) = -2\mu\tau\int_{-\infty}^{+\infty}\frac{i\epsilon\sin(2\varphi).y\zeta_T(iy) - \cos^2\varphi\zeta_T^2(iy) + \sin^2\varphi y^2}{(y-ia)\zeta_T(iy)[b-(iy\cos\varphi+\zeta_T(iy)\sin\tilde{\varphi})]}\,dy$$
$$= -2\mu\tau[\tilde{\nu}_T^2\cos^2\varphi J_8^T + i\epsilon\sin(2\varphi)J_6^T + \cos(2\varphi)J_7^T] \tag{B.57}$$

$$\mathcal{T}_7^{TV}(a,b) = \mu\tau\left(1-\frac{\tau^2}{\tilde{\nu}_T^2}\right)\int_{-\infty}^{+\infty}\frac{i\epsilon\cos\varphi.y\zeta_T(iy) + \sin\varphi y^2}{(y-ia)\zeta_T(iy)[b-(iy\cos\varphi+\zeta_T(iy)\sin\tilde{\varphi})]}\,dy$$
$$= -\mu\tau\left(1-\frac{\tau^2}{\tilde{\nu}_T^2}\right)[i\epsilon\cos\varphi J_6^T - \sin\varphi J_7^T] \tag{B.58}$$

$$\mathcal{T}_8^{TV}(a,b) = \mu\tau\left(1-\frac{\tau^2}{\tilde{\nu}_T^2}\right)\int_{-\infty}^{+\infty}\frac{\cos\varphi.\zeta_T(iy) - i\epsilon\sin\varphi y}{(y-ia)[b-(iy\cos\varphi+\zeta_T(iy)\sin\tilde{\varphi})]}\,dy$$
$$= \mu\tau\left(1-\frac{\tau^2}{\tilde{\nu}_T^2}\right)[\cos\varphi(J_7^T + \tilde{\nu}_T^2 J_8^T) + i\epsilon\sin\varphi J_6^T] \tag{B.59}$$

$$\mathcal{T}_9^{TV}(a,b) = -\mu(\tilde{\nu}_T^2-\tau^2)\int_{-\infty}^{+\infty}\frac{\epsilon\cos\varphi.\zeta_T(iy) - i\sin\varphi y}{(y-ia)\zeta_T(iy)[b-(iy\cos\varphi+\zeta_T(iy)\sin\tilde{\varphi})]}\,dy$$
$$= \mu(\tilde{\nu}_T^2-\tau^2)[\epsilon\cos\varphi J_3^T + i\sin\varphi J_5^T] \tag{B.60}$$

This concludes computation of coefficients of matrix $\mathbb{T}_{kl}$. It has been verified that all diverging terms that appear in integrals J_1^* to J_8^* compensate each other when the L, TH and TV terms are summed.

Acknowledgments

We would like to thank L. Fradkin for proof-reading our work and for her interesting remarks and suggestions.

Competing interests

We have no competing interests.

Funding Source

This research did not receive any specific grant from funding agencies in the public, commercial, or not-for-profit sectors.

References

[1] A. A. Sommerfeld. Asymtotische darstellung von formeln aus beugungstehorie des lichtes. *Journal für die reine und angewandte Mathematik.*, 158:199–208, 1928.

[2] A. D. Rawlins. Spherical wave diffraction by a rational wedge. Technical report, Department of Mathematics and Statistics, Brunel University, 1986.

[3] R. G. Rojas. Electromagnetic diffraction of an obliquely incident plane wave field by a wedge with impedance faces. *IEEE Transactions on Antennas and Propagation*, 36(7):956–970, 1988.

[4] P. Gerard and G. Lebeau. Diffusion d'une onde par un coin. *Journal of the American Mathematical Society*, 6(2):341–424, 1993.

[5] O. Lafitte. The wave diffracted by a wedge with mixed boundary conditions. *Mémoires de la SMF*, 1:1–167, 2002.

[6] V. M. Babich, M. A. Lyalinov, and V. E. Girkurov. *Diffraction theory: Sommerfeld-Malyuzhinets technique.* Alpha Science, 2008.

[7] J.-M. Bernard. On the diffraction of an electromagnetic skew incident wave by a non perfectly conducting wedge. *Annales Des Télécommunications*, 45(1-2):30–39, 1990.

[8] A. A. Ayzenberg. *Transmission-propagation operator theory and tip-wave superposition method for sub-salt shadow wavefield description*. PhD thesis, Norwegian University of Science and Technology, 10 2015.

[9] N. Favretto-Cristini, A.M. Aizenberg, B. Ursin, P. Cristini, and A. Tantsereva. Analysis of wave scattering from a viscoelastic layer with complex shape. *Journal of Computational Acoustics*, 25(3):1750023 (12 pages), 2017.

[10] V. Daniele. The Wiener-Hopf technique for impenetrable wedges having arbitrary aperture angle. *SIAM Journal on Applied Mathematics*, 63(3):1442–1460, 2003.

[11] V. G. Daniele and G. Lombardi. Wiener-Hopf solution for impenetrable wedges at skew incidence. *IEEE Transactions on Antennas and Propagation*, 54(9):2472–2485, 2006.

[12] M. A. Nethercote, R. C. Assier, and I. D. Abrahams. Analytical methods for perfect wedge diffraction: a review. *Wave Motion*, 93(102479), 2020.

[13] L. Knopoff. Elastic wave propagation in a wedge. *Wave Propagation in Solids, J. Miklowitz, ed., Amer. Soc. Mech. Engineers*, pages 3–43, 1969.

[14] J. B. Keller. Geometrical theory of diffraction*. *J. Opt. Soc. Am.*, 52(2):116–130, 02 1962. URL `http://www.osapublishing.org/abstract.cfm?URI=josa-52-2-116`.

[15] D. Bouche, F. Molinet, and R. Mittra. *Asymptotic Methods in Electromagnetics*. Springer, 1997.

[16] B. Lu, M. Darmon, L. J. Fradkin, and C. Potel. Numerical comparison of acoustic wedge models, with application to ultrasonic telemetry. *Ultrasonics*, 65:5 – 9, 2016. URL `http://www.sciencedirect.com/science/article/pii/S0041624X15002644`.

[17] V. H. Aristizabal, F. J. Velez, and J. D. Jaramillo. Efficient solution for the diffraction of elastic sh waves by a wedge: Performance of various exact, asymptotic and simplified solutions. *Soil Dynamics and Earthquake Engineering*, 95:9 – 16, 2017. URL `http://www.sciencedirect.com/science/article/pii/S026772611730091X`.

[18] V. Zernov, L. Fradkin, A. Gautesen, M. Darmon, and P. Calmon. Wedge diffraction of a critically incident gaussian beam. *Wave Motion*, 50 (4):708–722, 2013.

[19] M. Darmon, V. Dorval, A. Kamta-Djakou, L. J. Fradkin, and S. Chatillon. A system model for ultrasonic NDT based on the physical theory of diffraction (PTD). *Ultrasonics*, 64:115–127, 2016.

[20] L. J. Fradkin, M. Darmon, S. Chatillon, and P. Calmon. A semi-numerical model for near-critical angle scattering. *Journal of the Acoustical Society of America*, 139(1):115–127, 2016.

[21] V. Zernov, A. Gautesen, L. Fradkin, and M. Darmon. Aspects of diffraction of a creeping wave by a back-wall crack. *J. Phys. Conf. Ser.*, (353):12–17, 2012.

[22] S. Mahaut, G. Huet, and M. Darmon. Modeling of corner echo in ut inspection combining bulk and head waves effect. *Proceedings of the 35th Annual Review of Progress in Quantitative Nondestructive Evaluation; 35th Annual Review of Progress in Quantitative Nondestructive Evaluation*, 1096:73–80, 2009.

[23] L. Fradkin, A.K. Djakou, C. Prior, M. Darmon, S. Chatillon, and P.F. Calmon. The alternative Kirchhoff approximation in elastodynamics with applications in ultrasonic nondestructive testing. *The ANZIAM Journal*, page 1–17, 2020. doi: 10.1017/S1446181120000036.

[24] V. Dorval, S. Chatillon, B. Lu, M. Darmon, and S. Mahaut. A general Kirchhoff approximation for echo simulation in ultrasonic NDT. *AIP Conference Proceedings-American Institute of Physics*, 143, 2012.

[25] P.Y. Ufimtsev. *Fundamentals of the Physical Theory of Diffraction.* John Wiley & Sons, 2007.

[26] V. Zernov, L. Fradkin, and M. Darmon. A refinement of the Kirchhoff approximation to the scattered elastic fields. *Ultrasonics*, 52(7):830 – 835, 2012. URL `http://www.sciencedirect.com/science/article/pii/S0041624X11002149`.

[27] M. Darmon, V. Dorval, A. Kamta Djakou, L. Fradkin, and S. Chatillon. A system model for ultrasonic NDT based on the Physical Theory of Diffraction (PTD). *Ultrasonics*, 64:115 – 127, 2016.

[28] J. D. Achenbach, A. K Gautesen, and H. McMaken. *Ray methods for waves in elastic solids: with applications to scattering by cracks*. Pitman advanced publishing program, 1982.

[29] L. J. Fradkin and R. Stacey. The high-frequency description of scatter of a plane compressional wave by an elliptic crack. *Ultrasonics*, 50: 529–538, 2010.

[30] R. G. Kouyoumjian and P. H. Pathak. A uniform geometrical theory of diffraction for an edge in a perfectly conducting surface. *Proceedings of the IEEE*, 62(11):1448–1461, 11 1974. ISSN 0018-9219.

[31] A. Kamta-Djakou, M. Darmon, L. J. Fradkin, and C. Potel. The uniform geometrical theory of diffraction for elastodynamics: Plane wave scattering from a half-plane. *The Journal of the Acoustical Society of America*, 138:3272–3281, 11 2015.

[32] A. K. Gautesen. Scattering of an obliquely incident rayleigh wave in an elastic quarterspace. *Wave Motion*, 8(1):27–41, 1986.

[33] A. K. Gautesen. Scattering of a rayleigh wave by an elastic quarter space - revisited. *Wave Motion*, 35(1):91–98, 2002.

[34] B. V. Budaev. Diffraction of elastic waves by a free wedge. reduction to a singular integral equation. *Journal of Soviet Mathematics*, 57(3): 3087–3092, 1991. URL `http://link.springer.com/10.1007/BF01098973`.

[35] B. V. Budaev. Elastic wave diffraction by a wedge-shaped inclusion. *Journal of Mathematical Sciences*, 73(3):330–341, 1995. URL `http://link.springer.com/10.1007/BF02362817`.

[36] B. V. Budaev. *Diffraction by Wedges*. Longman Scientific & Technical ; Wiley, 1995.

[37] B. V. Budaev and D. B. Bogy. Rayleigh wave scattering by a wedge. *Wave Motion*, 22(3):239 – 257, 1995. URL `http://www.sciencedirect.com/science/article/pii/016521259500023C`.

[38] V. V. Kamotski, L. Ju. Fradkin, B. A. Samokish, V. A. Borovikov, and V. M. Babich. On Budaev and Bogy's approach to diffraction by the 2d traction-free elastic wedge. *SIAM Journal on Applied Mathematics*, 67(1):235–259, 2006. URL `https://doi.org/10.1137/050637297`.

[39] A. K. Gautesen and L. J. Fradkin. Diffraction by a two-dimensional traction-free elastic wedge. *SIAM Journal of Applied Mathematics*, 70: 3065–3085, 01 2010.

[40] R. K. Chapman, S. F. Burch, N. J. Colett, and L. J. Fradkin. Ultrasonic inspection of tilted defects using the 'corner effect' – modelling and experimental validation. *Insight - Non-Destructive Testing and Condition Monitoring*, 50:66–69, 02 2008.

[41] J.-P. Croisille and G. Lebeau. *Diffraction by an Immersed Elastic Wedge*, volume 1723. Springer, 01 2000.

[42] S. Chehade, A. Kamta-Djakou, M. Darmon, and G. Lebeau. The spectral functions method for acoustic wave diffraction by a stress-free wedge : theory and validation. *Journal of Computational Physics*, 377:200–218, 2018. URL `https://doi.org/10.1016/j.jcp.2018.10.040`.

[43] V. V. Kamotski and G. Lebeau. Diffraction by an elastic wedge with stress-free boundary: existence and uniqueness. *Proceedings of the Royal Society of London A: Mathematical, Physical and Engineering Sciences*, 462(2065):289–317, 2006. URL `http://rspa.royalsocietypublishing.org/content/462/2065/289`.

[44] S. Chehade, M. Darmon, and G. Lebeau. 2D elastic plane-wave diffraction by a stress-free wedge of arbitrary angle. *Journal of Computational Physics*, 394:532–558, 2019. URL `https://doi.org/10.1016/j.jcp.2019.06.016`.

[45] S. Chehade. *Modelling of the 3D scattering of elastic waves by complex structures for specimen echoes calculation. Application to ultrasonic NDT simulation.* PhD thesis, Université Paris-Saclay, 09 2019.

[46] V. A. Borovikov. *Uniform Stationary Phase method*. Institution of electrical engineers, 1994.

[47] D. Gridin. High-frequency asymptotic description of head waves and boundary layers surrounding the critical rays in an elastic half space. *Journal of the Acoustical Society of America*, 104(3):1188–1197, 1998.

[48] V. V. Kamotski. The incidence of the plane wave on an elastic wedge at a critical angle. *St. Petersburg Math. Journal*, 15(3):419–436, 2004.

[49] M. Darmon, A. Kamta-Djakou, S. Chehade, C. Potel, and L. Fradkin. Two elastodynamic incremental models: The incremental theory of diffraction and a huygens method. *IEEE Transactions on Ultrasonics, Ferroelectrics, and Frequency Control*, 66(5):998–1005, 2019.